

The *Spitzer* view of FR–I radio galaxies: on the origin of the nuclear mid–infrared continuum.

C. Leipski

Department of Physics, University of California, Santa Barbara, CA 93106
leipski@physics.ucsb.edu

R. Antonucci

Department of Physics, University of California, Santa Barbara, CA 93106

P. Ogle

Spitzer Science Center, California Institute of Technology, Mail Code 220-6, Pasadena, CA 91125
and

D. Whysong

National Radio Astronomy Observatory, P.O. Box O, Socorro, NM 87801

ABSTRACT

We present *Spitzer* MIR spectra of 25 FR–I radio galaxies and investigate the nature of their MIR continuum emission. MIR spectra of star–forming galaxies and quiescent elliptical galaxies are used to identify host galaxy contributions while radio/optical core data are used to isolate the nuclear non–thermal emission. Out of the 15 sources with detected optical compact cores, four sources are dominated by emission related to the host galaxy. Another four sources show signs of warm, nuclear dust emission: 3C15, 3C84, 3C270, and NGC 6251. It is likely that these warm dust sources result from hidden AGN of optical spectral type 1. The MIR spectra of seven sources are dominated by synchrotron emission, with no significant component of nuclear dust emission. In parabolic SED fits of the non–thermal cores FR–Is tend to have lower peak frequencies and stronger curvature than blazars. This is roughly consistent with the common picture in which the core emission in FR–Is is less strongly beamed than in blazars.

Subject headings: galaxies: active — galaxies: jets — galaxies: nuclei

1. Introduction

Large double radio sources come in two radio–morphological types. The more powerful type is the “classical double” or FR–II source, whose prototype is Cygnus A. This group has strong terminal “hotspots”, and generally one–sided arcsecond (kpc) scale. The other type, FR–Is like Centaurus A and M87, is lower in radio luminosity, double–jetted, and edge–darkened (Fanaroff & Riley 1974). These sources mostly

have symmetric kpc jets.

It has been known since the 1960s that some of these giant ($\gtrsim 100$ kpc) radio sources show powerful optical/UV continuum emission (called “Big Blue Bump”, or BBB) from a central point source. This optical/UV emission is generally identified as thermal radiation from dense matter accreting onto supermassive black holes. The gravitational potential energy of this infalling matter is thought to power much or all of the observed activity. Ob-

jects showing this strong optical/UV continuum and accompanying broad emission lines are classified as quasars and broad line radio galaxies (hereafter, “quasars”). On the other hand, double radio sources without these components are called (Narrow Line) Radio Galaxies (NLRGs).

Many FR–II NLRGs have hidden quasars detected by spectropolarimetry (e.g. Antonucci 1984; Ogle et al. 1997; Cohen et al. 1999) and recently also by their strong hot nuclear dust emission in the mid infrared (e.g. Meisenheimer et al. 2001; Haas et al. 2004; Shi et al. 2005; Ogle et al. 2006; Cleary et al. 2007; Tadhunter et al. 2007). Thus, many powerful radio galaxies contain quasars which are hidden from direct view by dusty equatorial tori – i.e. as expected in the “Unified Model” (Barthel 1989; Antonucci 1993; Urry & Padovani 1995).

The total light optical spectra of many FR–II NLRGs already indicate the presence of a “classical” AGN (those thought to accrete radiatively efficiently) by their high ionization emission line ratios (high ionization galaxies – HIG¹). Some FR–II RGs and most FR–Is, however, show only weak line emission of low ionization and are therefore classified as low ionization galaxies (LIGs). Here a luminous AGN (if present) has to be discovered at other wavelengths. Alternatively, these radio galaxies may simply lack a hidden quasar. A lack of a BBB means, according to current wisdom, a lack of a copious and radiatively efficient accretion flow. Historically such a situation was thought to require energy extraction from black hole rotation, and various mechanisms have been suggested for this (e.g. Begelman, Blandford, & Rees 1984). Alternatively in principle accretion power could make the jet, yet not radiate significantly. In such a case the BBB is present, but of low power compared to a (lobe–matched) quasar BBB.

In an optical imaging study of 3CR FR–I sources using *Hubble Space Telescope*, Chiaberge et al. (1999) report unresolved central compact cores (CCCs) in the centers of most observed galaxies. The correlation of optical (at $\sim 7000 \text{ \AA}$) compact cores and radio (at 6 cm) cores in flux and lu-

minosity is taken as evidence for their common origin as synchrotron emission from the base of a jet. Assuming that the base of the jet is found on scales *smaller* than any obscuring torus and considering the high detection rate of CCCs (85%) they argue that we see directly into the nucleus and thus no standard, geometrically thick torus can be present in most low–luminosity (FR–I) radio galaxies. Since no broad lines or strong BBB emission is observed there could also be no hidden, radiatively efficient AGN in those cases. However, e.g. Cao & Rawlings (2004) note that if the emission from the jet occurs on scales larger than that of the torus the absence (or presence) of a torus cannot be directly inferred from the observed nuclear jet components. In addition, high–resolution CO maps have revealed massive nuclear tori like those invoked in the standard unified model in the center of at least two FR–I radio galaxies: 3C31 (Okuda et al. 2005) and NGC 3801 (Das et al. 2005). These tori have high molecular masses ($>10^8 M_{\odot}$), with high molecular column densities and probably geometrically thick shapes.

From an UV imaging study Zirbel & Baum (2003) argue that the properties of FR–Is are consistent with the classic unification models and the existence of an obscuring torus: While BL Lac objects are well aligned sources, FR–I sources with nuclear UV components are at a critical angle for which a torus hides the nucleus but not the jet (or the latter greatly outshines the former). FR–Is without nuclear UV components are thought to have a larger viewing angle where a torus hides the central regions completely.

Recently, some of the compact optical cores discovered by Chiaberge et al. (1999) have been studied with imaging polarimetry revealing fairly large polarization ($< 11\%$) which further indicates their non–thermal origin, though such high polarizations can also result from scattering (Capetti et al. 2007).

In the X–rays, FR–I sources are dominated by weakly absorbed non–thermal jet components in most cases (e.g. Balmaverde et al. 2006b; Evans et al. 2006). They lack the powerful absorbed, accretion–related component of a strong AGN (associated with a luminous accretion disk and circumnuclear obscuring structure). In many FR–IIs the latter is found *in addition* to the

¹Although such objects are usually referred to as high excitation galaxies (HEGs) the term HIGs seems more appropriate because the distinction is primarily one of ionization and not excitation, as expected for photoionized gases.

non-thermal jet component (Evans et al. 2006). Thus, in FR–Is any non-jet accretion-related X-ray component carries much lower intrinsic AGN luminosities (10^{39} – 10^{41} ergs $^{-1}$) or else their detection is hampered by column densities of well above 10^{24} cm $^{-2}$. Also Wu et al. (2007) argue that the (soft) X-rays in their FR–I sample can be accounted for by jet emission only. We must note however that FR–Is with broad emission lines in the optical do exist (e.g. 3C120, Tadhunter et al. 1993; see also Antonucci 2002a for an anecdotal listing of such objects). Such broad-line FR–Is can extend up to quasar luminosities (Gower & Hutchings 1984; Blundell & Rawlings 2001; Heywood et al. 2007).

We here present a study of the mid-infrared properties of a sample of FR–I radio galaxies. The motivation is to possibly detect a hidden AGN by the reprocessed warm thermal dust emission as found in many FR–II radio galaxies (e.g. Ogle et al. 2006). And even in the case of exceptionally high extinction which attenuates also the MIR luminosity, spectral features that give clues on the thermal or non-thermal origin of the emission might still be detectable. On the other hand, the nuclear part of the MIR spectra bridges the gap in wavelength between the optical compact cores and the radio cores observed by Chiaberge et al. (1999). If there is in fact no hidden AGN and no obscuring structure to be found in FR–Is, the MIR spectra should agree with synchrotron core estimates.

2. Sample selection and observations

Our sample of FR–I radio galaxies was selected from the 3CR (Spinrad et al. 1985) catalog (about half of the sources are also included in the 3CRR²). We selected a tractable subset of lobe dominated sources with a flux limit of ~ 15 Jy at 178 MHz. To increase the sample size we added some very similar sources which were close to, but technically below, the flux cut off. We also observed two additional sources because they were of special interest: 3C189³ as well as IC 4296. See Tab. 1 for some basic data of the selected sources. We note that

²<http://3crr.extragalactic.info/>

³3C189 is only part of the 3C catalog (Edge et al. 1959) but not of the 3CR or the 3CRR catalogues. See e.g. Laing et al. (1983) for details on these samples.

our sample is not complete but can be considered representative for lobe dominated FR–I sources. No sources were lost by imposing scientifically relevant selections.

The morphological classification of the sources according to the Fanaroff–Riley scheme (Fanaroff & Riley 1974) was checked using radio maps from the literature (see Tab. 1 for references).

The objects were observed in low-resolution mode with IRS (Houck et al. 2004) on board *Spitzer Space Telescope* (Werner et al. 2004), mostly under pid–20525. Each source under this pid was observed in staring mode for a total of 960 sec, 1440 sec, 720 sec, and 480 sec in SL2, SL1, LL2, and LL1, respectively. After averaging all the cycles at one nod position we subtracted the off-order frames to remove the background. The resulting images were cleaned of residual rogue pixels and cosmic rays using IRSCLEAN. The SPICE software was used to calibrate and extract one dimensional spectra. The extracted spectra from the two nod positions were then averaged and data from the different modules were combined into a single spectrum. Due to the larger slit width in LL (10.7" in LL versus 3.7" in SL), multiplicative factors (< 1.5) were applied to the SL modules where necessary in order to match the flux levels.

Spectra for additional FR–I sources not observed under pid–20525 (see Tab. 1, lower part) were also retrieved from the archive and were subject to the same procedures.

3. The Spitzer spectra

In Figures 1 and 2 we present the rest frame MIR spectra for our FR–I core sample and the supplemental objects. Because for 3C15 and 3C29 the SL modules of IRS suffer from saturated peak-up areas we present their spectra separately in Fig. 3. Statements on the spectral behavior of the individual sources refer to the figures where their observed spectra are shown (Figs. 1 and 2) and are thus considered in terms of F_{ν} . All sources in our sample have been detected except for 3C403.1 which was not detected in either SL or LL.

3.1. The main sample

3C31 (NGC 383) This source shows very strong PAH emission and the MIR spectrum is

Table 1: The Sample.

Object	alt. name	z	F _{178 MHz} Jy	total ref ^a	F _{5 GHz} mJy	core ref ^a	F _{CCC} ^b μJy	λ _{CCC} filter	map ref ^a	spec ref ^a
3C15		0.073000	17.2	42	32	25	38	F160W	22	48
3C29		0.045031	16.5	42	93	24	10	F702W	24	48
3C31	NGC 383	0.017005	18.3	43	92	12	29	F702W	19	48
3C66B		0.021258	26.8	43	182	12	97	F702W	14	48
3C76.1		0.032489	13.3	43	10	37	21	48
3C83.1	NGC 1265	0.025137	29.0	43	25	27	3	F702W	27	48
3C129		0.020800	51.1	44	34	38	36	48
3C189	NGC 2484	0.040828	7.4	45	195	13	76	F814W	7	1
3C264	NGC 3862	0.021718	28.3	43	200	12	248	F791W	41	28
3C270	NGC 4261	0.007465	56.5	42	308	24	11	F791W	9	33
3C272.1	M 84	0.003536	21.1	43	180	12	139	F814W	18	48
IC 4296		0.012465	16.8	46	297	24	524	F160W	24	40
3C293		0.045034	13.8	43	100	12	5	34
3C317		0.034457	53.4	42	391	24	23	F814W	6	48
NGC 6251		0.024710	11.6	43	350	16	191	F812W	30	23
3C386		0.016885	26.1	43	14	32	2301	F702W	21	48
3C403.1		0.055400	14.7	42
3C424		0.126988	15.9	42	18	8	3	48
3C465	NGC 7720	0.030221	41.2	43	270	12	36	F702W	10	11
3C84	NGC 1275	0.017559	66.8	43	3100	26	3489	F702W	29	48
3C120		0.033010	7.4	45	1970	39	31	33
3C218	Hyd A	0.054878	225.7	46	217	24	35	40
3C274	M 87	0.004360	1144.5	43	4000	12	894	F814W	15	48
BL Lac		0.068600	~ 2.5 ^c	47	~ 4.0 ^c	2	20
E1821+643		0.297000	~ 0.5	47	8.0	4	4	17

^aReferences for total radio fluxes, radio core fluxes, radio maps, and optical spectra, respectively.

^bData taken from Chiaberge et al. (1999) except for 3C189 (Capetti et al. 2002), IC4296 (Balmaverde et al. 2006a), and NGC 6251 (Chiaberge et al. 2003). Data on 3C15 provided by R. Baldi (private communication).

^cThe flux of *only* the extended emission is 29 mJy at 20 cm (Antonucci 1986) which correspond to ~ 151 mJy at 178 MHz (using $\alpha = -0.8$; $S \propto \nu^\alpha$). For the variable 5 GHz core flux we here give the average of all measurements available from NED.

References. — (1) SDSS; (2) Antonucci 1986; (3) Black et al. 1992; (4) Blundell & Rawlings 2001; (5) Bridle et al. 1981; (6) Burns 1990; (7) Capetti et al. 1993; (8) Chiaberge et al. 1999; (9) Condon & Broderick 1988; (10) Condon et al. 1991; (11) De Robertis & Yee 1990; (12) Giovannini et al. 1988; (13) Giovannini et al. 2005; (14) Hardcastle et al. 1996; (15) Hines et al. 1989; (16) Jones et al. 1986; (17) Kollatschny et al. 2006; (18) Laing & Bridle 1987; (19) Laing et al. 2008; (20) Lawrence et al. 1996; (21) Leahy & Perley 1991; (22) Leahy et al. 1997; (23) Miley & Osterbrock 1979; (24) Morganti et al. 1993; (25) Morganti et al. 1999; (26) Taylor et al. 2006; (27) O’Dea & Owen 1986; (28) Owen et al. 1996; (29) Pedlar et al. 1990; (30) Perley et al. 1984; (31) Simpson et al. 1996; (32) Strom et al. 1978; (33) Tadhunter et al. 1993; (34) Tadhunter et al. 2005; (35) Taylor et al. 1990; (36) Taylor et al. 2001; (37) Vallee 1982; (38) van Breugel & Jägers 1982; (39) Walker et al. 1987; (40) Wills et al. 2004; (41) see <http://www.jb.man.ac.uk/atlas/>; (42) Kellermann et al. (1969), on Baars et al. (1977) scale using Laing & Peacock (1980); (43) taken from <http://3crr.extragalactic.info/>; (44) estimated using GMRT measurements (Lal & Rao 2004); (45) Kuehr et al. 1981; (46) estimated using the 160 MHz flux (Kuehr et al. 1981) and $\alpha = -0.8$; (47) estimated from low frequency measurements in NED; (48) Buttiglione et al. 2009

likely to be dominated by emission related to star formation.

A massive molecular gas disk has been detected in CO in this object (Okuda et al. 2005).

3C66B This source shows increasing flux towards the shortest wavelengths observed (starting at around 8 μm) indicating a dominant contribution from the stellar component of the host galaxy

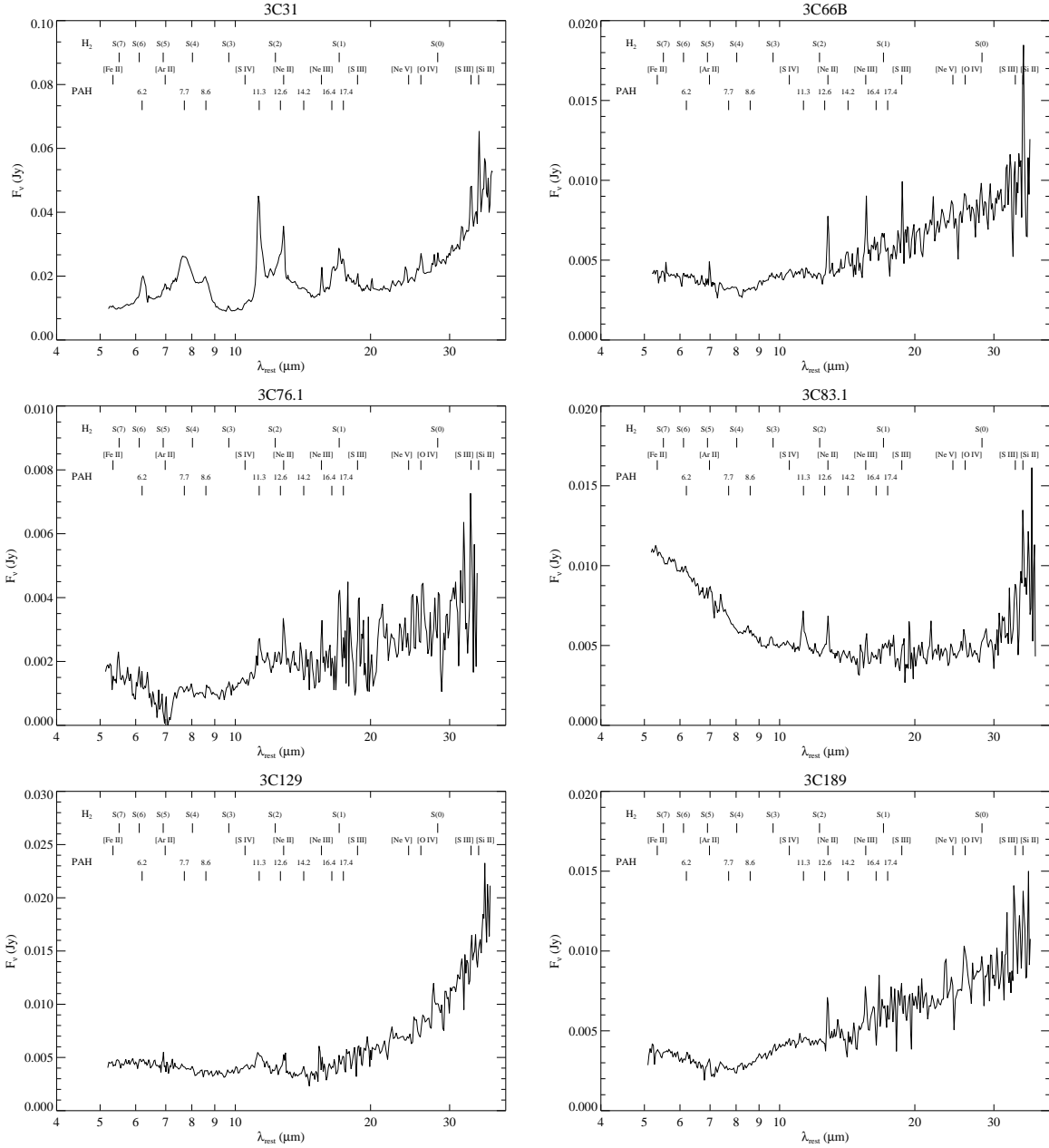


Fig. 1.— Observed MIR spectra of the FR-I sources. Flux in Jy is plotted over the rest frame wavelength in μm .

at these wavelengths. A weak silicate feature in emission can be seen around $9.7\ \mu\text{m}$ as well as significant red continuum at longer wavelengths. Atomic line emission from low ionization species is detected but no PAH features.

3C76.1 While this source is clearly detected

(as seen from the 2-D frames) it has low flux and shows a noisy spectrum. No spectral features can be securely identified. The spectrum shows slowly increasing flux towards longer wavelengths, starting at around $15\ \mu\text{m}$.

3C83.1 (NGC 1265) Emission from the

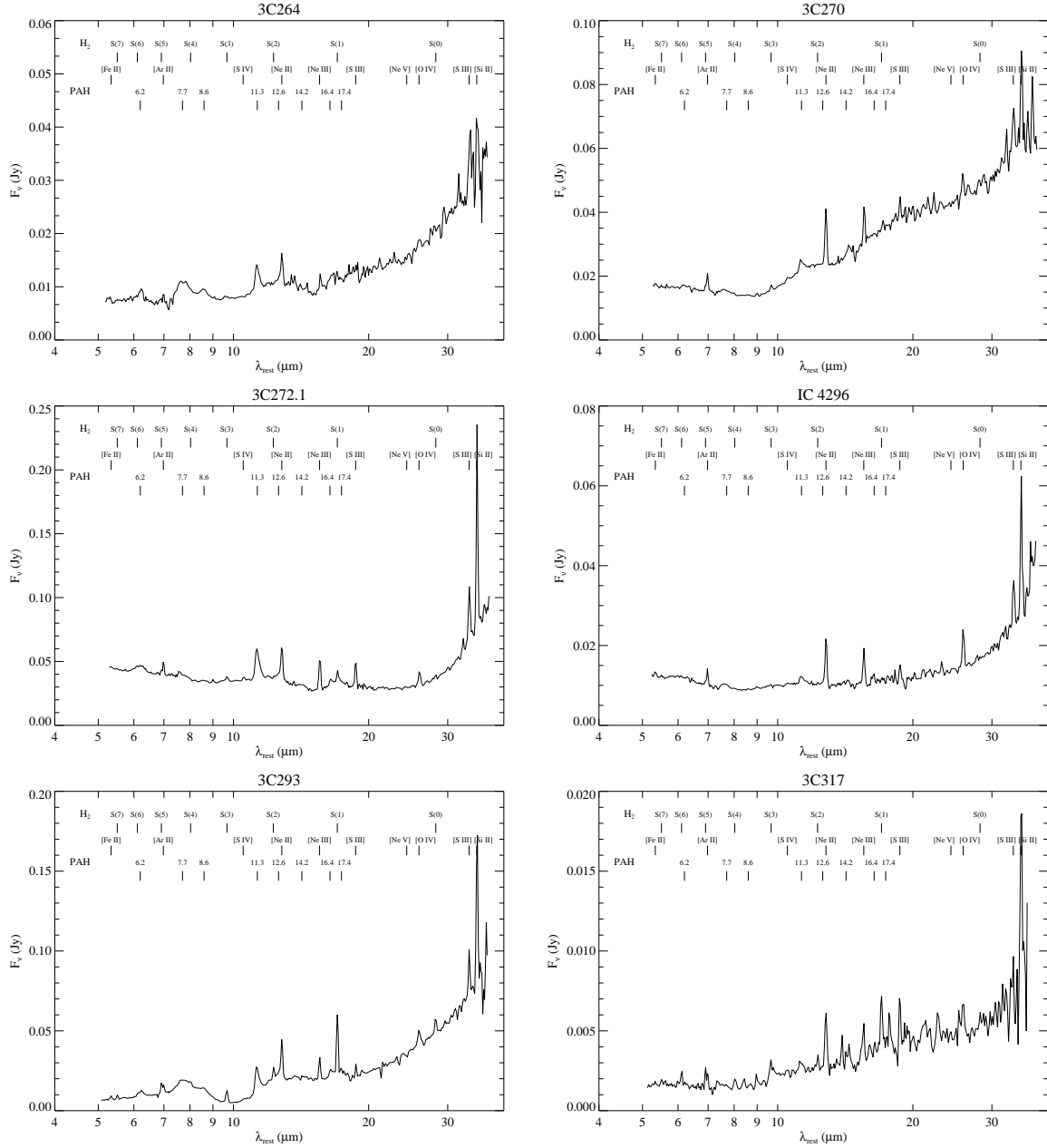


Fig. 1.— *continued*

host galaxy stellar population dominates this source up to $\sim 15 \mu\text{m}$ where the spectrum starts to flatten in flux. PAH emission at $11.3 \mu\text{m}$ and atomic emission from [Ne II] at $12.8 \mu\text{m}$ are clearly detected. The ratio between the PAH features at $7.7 \mu\text{m}$ and $11.3 \mu\text{m}$ appears very small compared to e.g. 3C31 (see § 4.1).

3C129 Here the stellar emission again dominates below $\sim 10 \mu\text{m}$ and for $\lambda > 15 \mu\text{m}$ strong MIR continuum emission is observed. We also detect weak silicate emission and PAHs at $11.3 \mu\text{m}$.

3C189 (NGC 2484) This source appears very similar to 3C66B in the MIR spectrum with a distinct stellar component at short wavelengths,

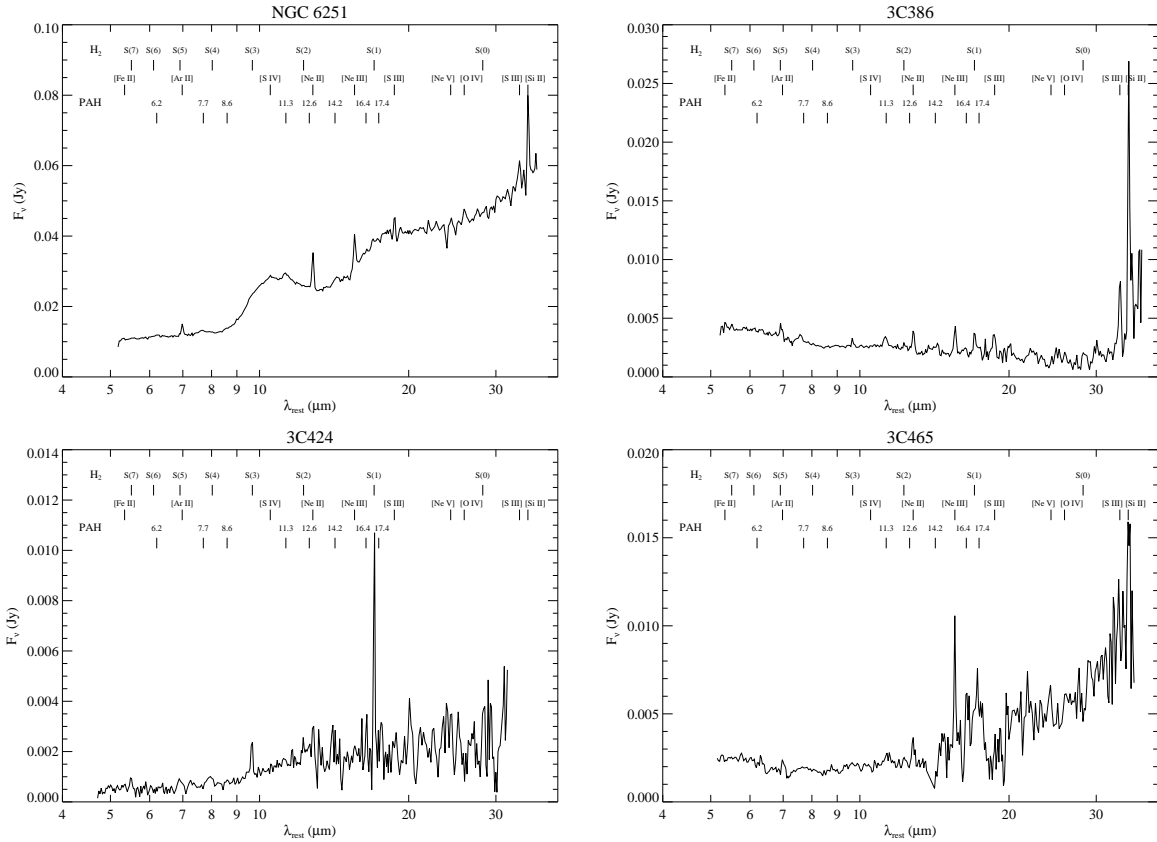


Fig. 1.— *continued*

weak silicate emission around $9.7 \mu\text{m}$, red continuum emission for $\lambda > 10 \mu\text{m}$, and no PAHs.

3C264 (NGC 3862) Strong PAH features are detected in this source which argues for a considerable, if not dominant, contribution from emission related to star formation. In fact, the steep continuum at $\lambda > 20 \mu\text{m}$ might well be associated with star formation. At the shortest wavelengths some minor contributions from the host galaxy stars can be identified.

3C270 (NGC 4261) A weak silicate feature and weak PAH emission is detected. While the blue spectral slope towards shorter wavelengths indicates contributions by stellar emission, a strong red continuum is observed for $\lambda > 10 \mu\text{m}$. In combination with the relatively weak PAH emission this continuum emission is not likely to originate from star-forming activity only.

3C272.1 (M 84 – NGC 4374) A very unusual spectrum which has a blue slope up to

$\sim 20 \mu\text{m}$ and shows a very steep red slope at $\lambda > 30 \mu\text{m}$. Strong PAH emission is observed, but as in the case of 3C83.1 the $7.7 \mu\text{m}$ to $11.3 \mu\text{m}$ ratio appears very small. Several atomic emission lines are detected, among them [O IV], a relatively high ionization line which can, however, also be found in star-forming galaxies (e.g. Smith et al. 2007).

IC 4296 Somewhat similar in appearance to 3C272.1 the continuum shows a red slope for $\lambda > 20 \mu\text{m}$ which steepens for $\lambda > 30 \mu\text{m}$. Weak PAH emission and strong atomic line emission is detected. The [O IV] emission line has much larger equivalent width than in 3C272.1 although the relative contributions from star formation to the spectrum, as traced by the PAHs, is apparently lower.

3C293 The MIR spectrum of this object is clearly dominated by star formation. The strong PAH features and the shape of the red continuum are very similar to what is seen in local star-

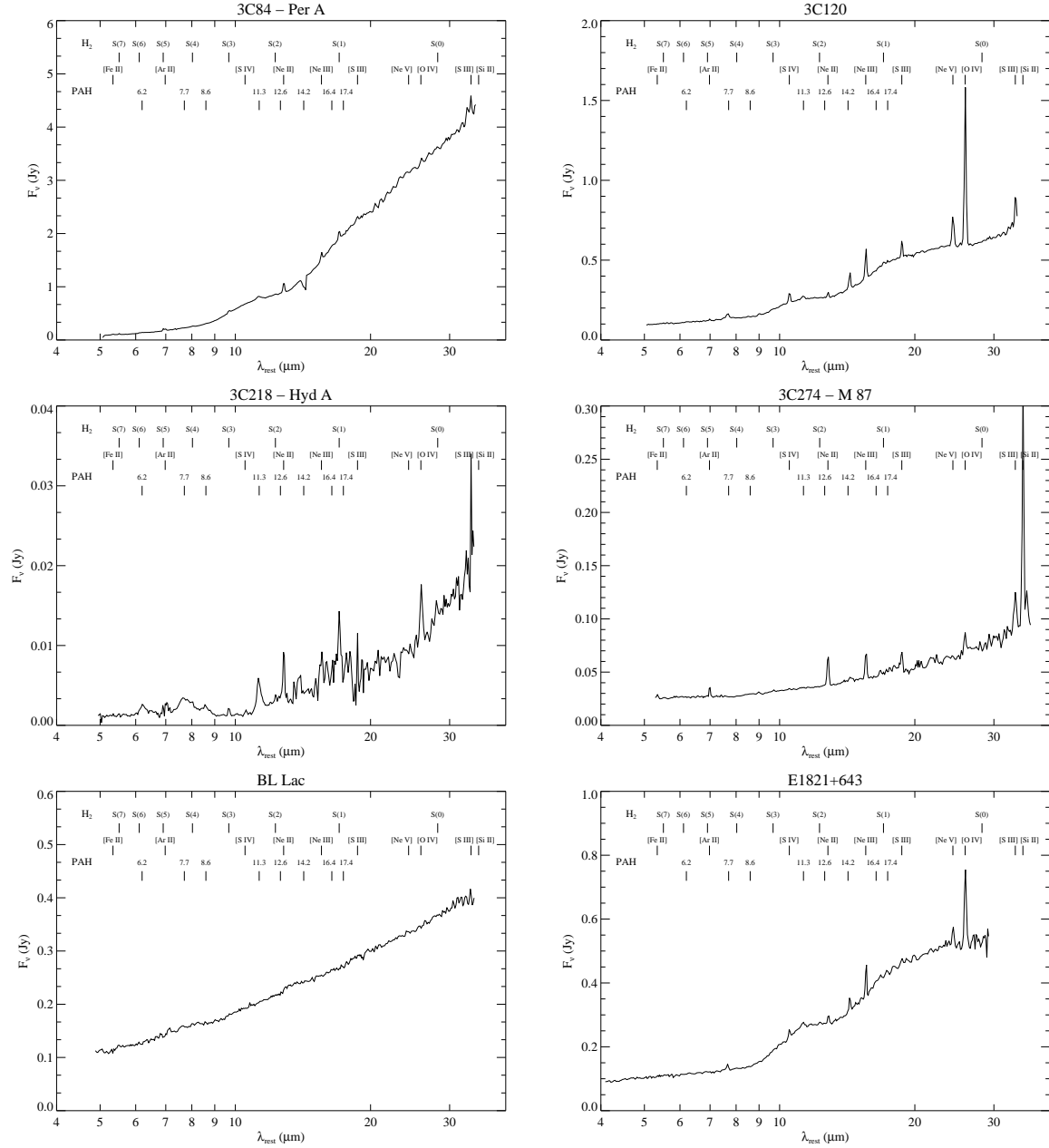


Fig. 2.— Observed MIR spectra of the supplemental objects. Again we plot the flux in Jy over the rest frame wavelength in μm .

forming galaxies (e.g. Smith et al. 2007). Notably, we also detect several rotational transitions from molecular hydrogen in emission (Ogle et al., in preparation).

3C317 This source shows a blue slope at the lowest wavelengths suggestive of stellar emission.

Starting at around $10 \mu\text{m}$ the spectrum turns to a red, but not very steep slope. We do not detect significant PAH features and [Ne II] $\lambda 11.3 \mu\text{m}$ is the strongest atomic emission line. We do, however, detect faint emission from molecular hydrogen from S(1) up to at least S(6) (Ogle et al., in

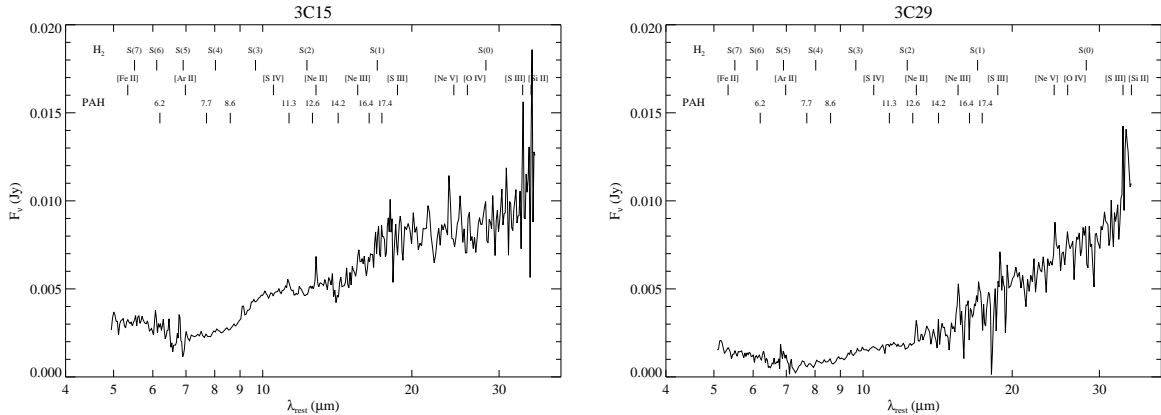


Fig. 3.— The MIR spectra of 3C15 (left) and 3C29 (right).

preparation).

NGC 6251 Strong silicate emission at $9.7\ \mu\text{m}$ and $18\ \mu\text{m}$ is detected as previously noted in Ogle et al. (2007). Strong atomic and weak PAH emission can also be seen.

3C386 This source shows a very starlight-dominated, blue continuum throughout the whole covered wavelength range. Some PAH features (e.g. $7.7\ \mu\text{m}$ and $11.3\ \mu\text{m}$) and atomic lines (e.g. [Ne II] $\lambda 12.8\ \mu\text{m}$ and [Ne III] $\lambda 15.6\ \mu\text{m}$) are present as well as weak molecular hydrogen emission. Simpson et al. (1996) tentatively detected a broad $H\alpha$ line in the optical and Madrid et al. (2006) find that a foreground star falls on top of the nucleus for this galaxy (previously also noted by Lynds 1971).

3C424 The continuum emission is rather weak in this source but we detect it in all orders. The most notable feature in this spectrum is the exceptionally bright S(1) emission line from molecular hydrogen. Several other H_2 emission lines can be identified as well.

3C465 (NGC 7720) While the presence of stellar emission can be identified at short wavelengths, the spectrum shows a prominent red slope for $\lambda > 20\ \mu\text{m}$. Some atomic emission lines are detected on top of the rather noisy continuum and no significant PAH features (besides a possible detection of a weak $11.3\ \mu\text{m}$ feature) are found. Inspection of the 2-D spectral frames confirms that the source is detected in all orders, but especially in LL2 ($\sim 15 - 20\ \mu\text{m}$) it is of very low S/N.

3.2. The supplemental sample

In Fig. 2 we show the spectra of the FR-I sources that do not belong to our initial sample. We use them here to demonstrate the diversity of MIR spectra seen for FR-I sources.

3C84 (Per A – NGC 1275) This source is highly core dominated in the radio (Pedlar et al. 1990). In the MIR, however, a strong thermal spectrum, including weak silicate emission and a steepening around $12\ \mu\text{m}$ is observed. It appears very similar in shape to the spectrum of the classical hidden AGN source 3C405 (=Cyg A; Fig 4) but the continuum appears much stronger in 3C84 relative to the emission lines.

3C120 This source is the only 3C FR-I source in our sample where an AGN is already clearly visible at optical wavelengths as traced by broad emission lines and a blue optical/UV spectrum (Tab.1). The *Spitzer* spectrum reflects this by showing silicate emission at $9.7\ \mu\text{m}$ and $18\ \mu\text{m}$, a rather flat continuum compared to sources like 3C84 and 3C405 and strong [Ne V] and [O IV] emission similar to the MIR spectra of typical type-1 AGN (e.g. Weedman et al. 2005; Buchanan et al. 2006).

3C218 Hydra A is the only source in our sample which is morphologically clearly a FR-I but with an $178\ \text{MHz}$ luminosity that places it among the FR-IIs. Optically a low ionization galaxy (Tab.1) the MIR spectrum shows PAH emission and [O IV] is also detected. Overall the spectrum looks quite similar to sources dom-

inated by star formation in the MIR (e.g. 3C31, 3C293). However, here the continuum starts rising already at around 10 to 12 μm while for the other star-forming sources such a steepening in the continuum is observed around $\sim 20 \mu\text{m}$ (Smith et al. 2007). Thus it might have a warmer dust component or stronger non-thermal core contributions.

3C274 (M 87 – Vir A – NGC 4486) The MIR spectrum of M 87 shows a rather flat slope overlaid with some line emission from generally low ionization species (except for some weak [O IV] emission). At short wavelengths some contributions from the host galaxy can be identified and there is even some shallow silicate emission detected. For this source high-resolution ground based MIR flux measurements at $\sim 0.5''$ resolution are also available (Perlman et al. 2001; Whyson & Antonucci 2004).

BL Lac As is common to sources in the class of objects named after this prototype, BL Lac is dominated by Doppler boosted synchrotron emission at least from the radio through the optical. The MIR spectrum is also dominated by this synchrotron emission and shows a virtually featureless power-law continuum ($\alpha \sim -0.7$). The diffuse radio emission suggests a relatively weak FR-I source (Antonucci 1986). We show this object to illustrate a purely non-thermal spectrum.

E1821+643 This source was first classified as a radio-quiet QSO, but discovered in a survey at low radio frequencies (Lacy et al. 1992). Deep radio imaging, however, revealed a ~ 300 kpc FR-I radio structure associated with this source (Blundell & Rawlings 2001). Being a broad-line object the MIR spectrum looks quite similar to those of most other quasars or broad-line objects (e.g. 3C120). We clearly detect silicate emission at $9.7 \mu\text{m}$ and a weak emission feature at $18 \mu\text{m}$. We also detect [Ne V] emission and weak PAH emission (e.g. at $11.3 \mu\text{m}$). The continuum longward of $\sim 10 \mu\text{m}$ is redder than for 3C120 but not as red as for hidden AGN sources like Cyg A.

In Fig. 3 we present the MIR spectra of 3C15 and 3C29. The spectra of these objects suffer from “spill-over” due to saturated peak-up areas. Therefore the flux levels and the slopes in the SL modules are likely to be compromised. It is notable, however, that both sources clearly show a red continuum at wavelengths greater than $15 \mu\text{m}$

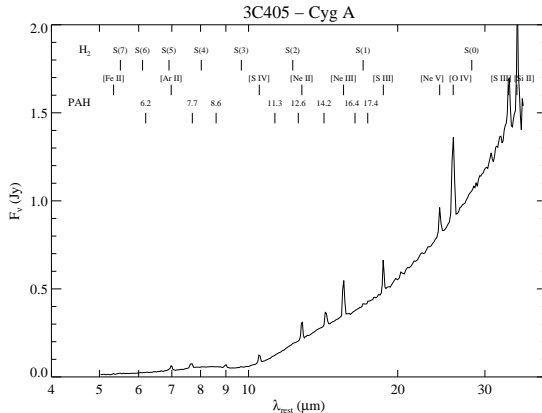


Fig. 4.— Observed MIR spectrum of 3C405, a prototypical hidden AGN source.

but no significant PAH emission. Since the red continuum is detected in the LL orders it is not an artifact of the spill-over.

4. MIR emission in FR-I radio galaxies

In this paper we study the nuclear MIR emission of FR-I radio galaxies and try to determine its properties and possible origins. Components considered are i) synchrotron emission from a non-thermal core, ii) warm dust emission resulting from AGN heating, iii) dust heated by star formation as traced by PAH features, and iv) stellar emission (photospheric emission plus dust emission associated with the circum-stellar envelopes of AGB stars). We often summarize contributions iii and iv as processes from the host galaxy. We use the term “nuclear” to address central emission related directly to an AGN⁴.

In the framework of models which favor the absence of nuclear dust with high covering factors in FR-I sources, the MIR spectra should consist of a combination of non-thermal emission due to a nuclear synchrotron source and more extended emission related to processes in the host galaxy. The warm/hot dust component related to an AGN should be missing or of very low luminosity. In

⁴We note that the definite test for the nuclear origin of the detected MIR emission would be high spatial resolution MIR imaging in order to compare the fluxes of any sub-arcsec nuclear point sources with the *Spitzer* fluxes (see e.g. Whyson & Antonucci (2004) for a discussion of the contrasting results on M 87 and Cen A).

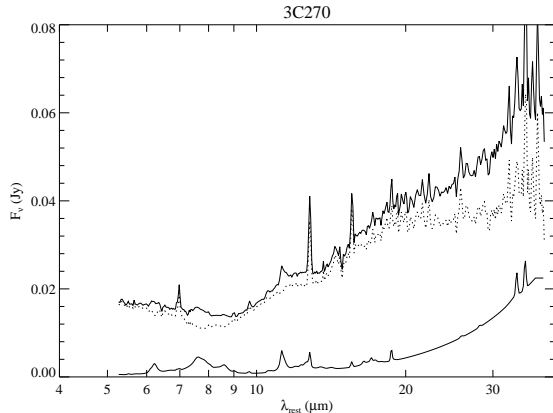


Fig. 5.— 3C270 as an example for the subtraction of the star-forming template (thin solid line) which is scaled to remove the $11.3\ \mu\text{m}$ PAH feature. The spectrum on the top is the total observed spectrum while the dotted line shows the star-formation corrected spectrum (note the absence of the $11.3\ \mu\text{m}$ PAH feature).

order to explore any nuclear MIR emission in FR-I sources, we will here test this scenario by successively identifying contributions from different mechanisms to the MIR spectra.

4.1. Contributions from star formation

Due to the large slit width of IRS ($3.7''$ and $10.7''$ for SL and LL, respectively) contributions from the host galaxy (star formation and stellar emission) to the MIR continuum can be significant and even dominant. We need to correct our spectra for these host galaxy contributions in order to explore any additional nuclear MIR emission.

Because emission related to star formation has intrinsically a red spectral slope it cannot be distinguished easily from the synchrotron core emission or AGN heated dust. Therefore, in order to securely identify any synchrotron or AGN dust components in the observed MIR spectra, emission from star formation needs to be corrected for. As an indicator for star-forming contributions we here use the PAH features which are commonly observed in the spectra of star-forming galaxies and are a well known tracer of star-formation activity. Only if PAHs are detected do we correct the spectra for emission related to star formation. No significant PAH emission usually indicates negli-

gible continuum contribution from star formation compared to other processes.

In the case of detected PAH emission we chose to subtract appropriately scaled average star-formation template spectra taken from Smith et al. (2007). We used the template with the reddest MIR/FIR slope which was still in accordance with the data after scaling, thus being conservative about any residual emission. The template was scaled to the $11.3\ \mu\text{m}$ PAH feature which is strong, largely free of contaminations by atomic emission lines, and close to wavelengths where AGN related emission usually has a large contribution. The star-forming template was scaled in such a way that, after subtraction, the $11.3\ \mu\text{m}$ PAH feature is removed from our FR-I spectrum (see Fig. 5 for illustration). In Tables 2 and 3 we give estimates for the percentage contributions from star formation to the observed MIR flux at $15\ \mu\text{m}$ and $30\ \mu\text{m}$.

While this strategy works well for many of our sources, subtraction of the star-formation template (scaled to the $11.3\ \mu\text{m}$ PAH feature) leaves a clear depression at the location of the $7.7\ \mu\text{m}$ feature for 3C83.1 and 3C272.1. This cannot be explained by the shape of stellar emission and argues for a very low $7.7\ \mu\text{m}/11.3\ \mu\text{m}$ PAH ratio in these FR-I galaxies (Fig. 6). Apart from the low PAH ratio both spectra can be explained by a combination of processes in the host galaxy. We detect no significant nuclear continuum (but see §4.3).

Such low PAH ratios have already been noted in local (early-type) galaxies (Kaneda et al. 2005; Smith et al. 2007; Kaneda et al. 2008). Sources with MIR continua dominated by star formation usually show no large variation in the $7.7\ \mu\text{m}$ to $11.3\ \mu\text{m}$ ratio (Brandl et al. 2006; Smith et al. 2007) and similar star-formation dominated PAH ratios have been found in luminous radio-quiet and radio-loud AGN (Shi et al. 2007b). In absence of strong contributions from star formation, spectra with unusual $7.7\ \mu\text{m}/11.3\ \mu\text{m}$ values can be observed. Interestingly, most sources with such low PAH ratios show low-luminosity AGN activity (Smith et al. 2007). Consistent with this, Sturm et al. (2006) have shown that IR-faint LINERs (LINERs without much star formation) show these unusual PAH ratios, while IR-luminous ($L_{\text{IR}}/L_B \gtrsim 1$ with L_{IR} being the $8 - 1000\ \mu\text{m}$ luminosity) LINERs have PAH ratios

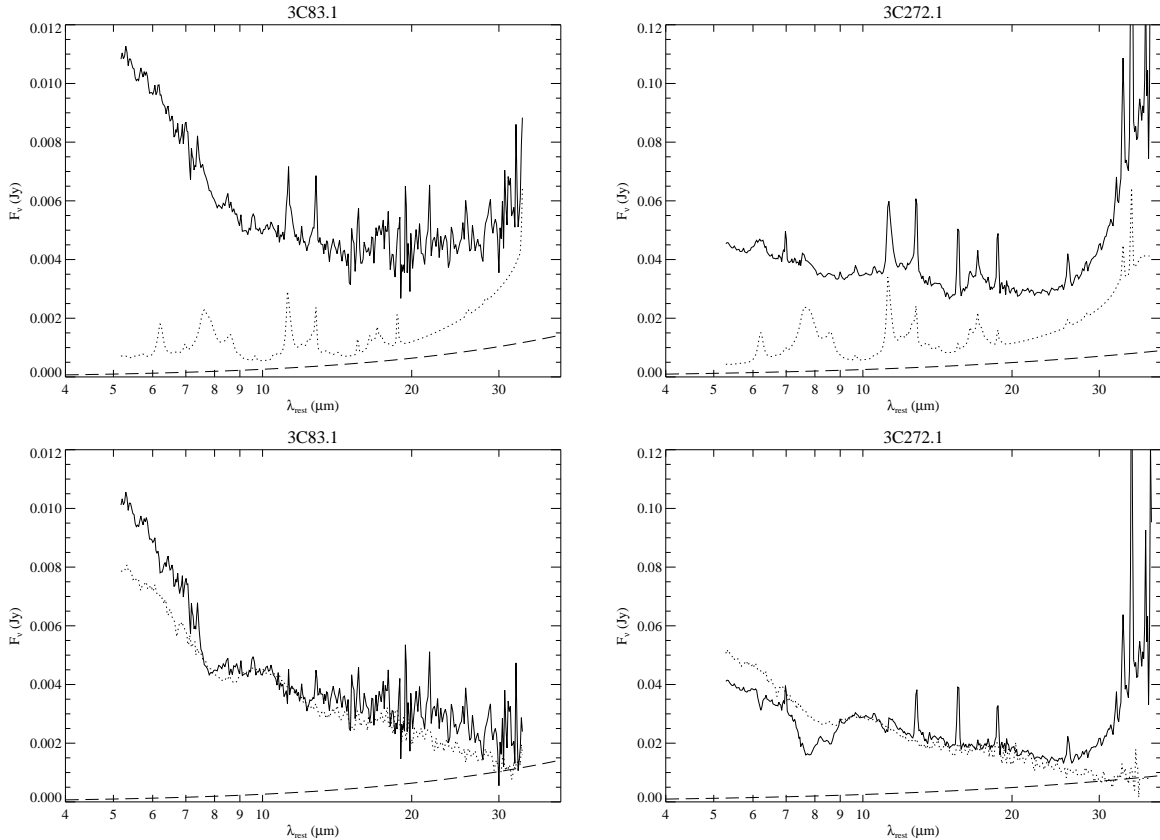


Fig. 6.— The unusual PAH ratios in 3C83.1 (*left*) and 3C272.1 (*right*). The top panel shows the observed spectrum with the star-formation template scaled to the $11.3\ \mu\text{m}$ PAH feature. The bottom panel shows the results of the subtraction and the scaled spectrum of an early-type galaxy (NGC 1549). Approximate contributions from the synchrotron core (§4.4) are shown as long-dashed lines.

similar to starburst galaxies. In the former cases it appears that the nuclear source powers most of the measured PAH emission. The harder spectrum could potentially lead to the destruction of the carriers of the $7.7\ \mu\text{m}$ band or to the preferential excitation of the $11.3\ \mu\text{m}$ PAH, thus explaining the observed relative decrease in the $7.7\ \mu\text{m}$ feature (Smith et al. 2007; Kaneda et al. 2008, and references therein). This could in principle indicate that the PAHs in 3C83.1 and 3C272.1 are not excited by star formation but by (low-luminosity) AGN activity instead. Any corrections made to the spectrum by the subtraction of a star-forming template would thus remove MIR continuum emission which is in fact powered by the AGN.

4.2. Contributions from stellar emission

Recall that we have already seen in the spectra (Fig. 1) that contributions from stellar emission of the host galaxy can be substantial, particularly at shorter wavelengths. Most or all of our FR-I sources reside in elliptical galaxies (e.g. Govoni et al. 2000; Madrid et al. 2006). The MIR spectra of early-type galaxies generally show blue colors throughout the IRS wavelength range (e.g. Bressan et al. 2006; Kaneda et al. 2008) and even if moderate amounts of residual star formation are observed, the blue spectral slopes of the stellar emission can remain dominant in the total spectrum (Kaneda et al. 2008). This is supported by the fact that the SEDs of typical early-type galaxies without signs for considerable star formation usually show a blue IR slope that, due

to emission from cold dust, turns over into a red slope at wavelengths beyond the IRS coverage (e.g. Dale et al. 2005; Kaneda et al. 2007; Temi et al. 2007). Therefore, the stellar contributions in our MIR spectra will have opposite spectral slope compared to any underlying synchrotron core or warm dust emission.

As shown by e.g. Bressan et al. (2006) the MIR spectra of non-active early-type galaxies can be well explained by including the dusty atmospheres and envelopes of AGB stars into stellar evolution models. The emission from dust produced in the atmospheres of AGB stars accounts for excess continuum emission over the long-wavelength quasi Rayleigh-Jeans extrapolation of late-type stars as well as for the presence of silicate emission in the spectra of early-type galaxies.

We estimate contributions from the stellar population by using the observed spectrum of a quiescent elliptical galaxy which is scaled to the blue part of the spectra ($\sim 5 - 8 \mu\text{m}$). For a template we chose the quiescent early-type galaxy NGC 1549 which is fairly bright at MIR wavelengths, does not show any PAH or atomic line emission, and has full IRS low-resolution coverage (Kaneda et al. 2008). We obtained the data for NGC 1549 from the *Spitzer* archive and extracted a spectrum following the procedures described in Kaneda et al. (2008). In Tables 2 and 3 we list estimated percentage contributions of the stellar component to the observed MIR flux at two wavelengths.

4.3. Spectral components in the MIR

After the subtraction of the star-forming template in the way described above and after considering the stellar host galaxy emission we recognize basically two types of spectra:

(1) sources where the observed MIR emission can be accounted for by processes in the host galaxy.

The spectra are either dominated by star formation (3C31, 3C218, 3C264, 3C293) or the observed MIR emission can be explained by a combination of stellar and star-forming contributions (i.e. after the subtraction of the star-forming template the residual spectrum is largely consistent with stellar emission from an early type galaxy; 3C76.1, 3C386; Fig. 13).

(2) objects which show significant residual emission at wavelengths longer than $\sim 8 \mu\text{m}$ with a red spectral slope.

Because even star formation and stellar emission combined cannot explain these residual continua they must originate from other processes, for example warm (few hundred K) dust emission or non-thermal synchrotron emission. In some of the sources where residual continuum emission at $\lambda > 8 \mu\text{m}$ could be identified we also detect PAHs (3C84, 3C120, 3C129, 3C270, IC4296, NGC 6251, E1821+643; Figs. 13,14), but the equivalent widths of these features are generally small. For many sources only red continuum emission at $\lambda > 8 \mu\text{m}$ (plus possibly stellar host galaxy emission) was detected (3C15, 3C29, 3C66B, 3C189, 3C274, 3C317, 3C424, 3C465, BL Lac). No significant PAH emission can be seen in their spectra.

As mentioned above in the case of 3C83.1 and 3C272.1 we cannot without doubt attribute the PAH emission to star formation. We count these objects as host-dominated sources, an interpretation which is supported by the shape of their MIR continuum (Fig. 6), but we emphasize that we cannot be sure at this point if the PAH emission is excited by star formation or (low-luminosity) AGN activity.

4.4. Comparison with synchrotron prediction

Since it has been proposed that non-thermal emission might be a major, if not dominant constituent of the MIR emission in FR-I sources, we also analyze the MIR spectra in the framework of their (nuclear) SEDs. As a comparison for the synchrotron core emission we chose to use well observed blazars and related objects because they represent nearly pure synchrotron emission.

It has been shown that, globally over a large frequency interval, the strongly beamed core emission of blazars can be well approximated by a parabolic function in $\log F_\nu$ vs. $\log \nu$ (e.g. Landau et al. 1986). Following these authors we here utilize a function of the form

$$\log F_\nu = C + (\log \nu - B)^2 / 2A \quad (1)$$

to represent the underlying beamed emission from the base of the jet (C is the log of the peak

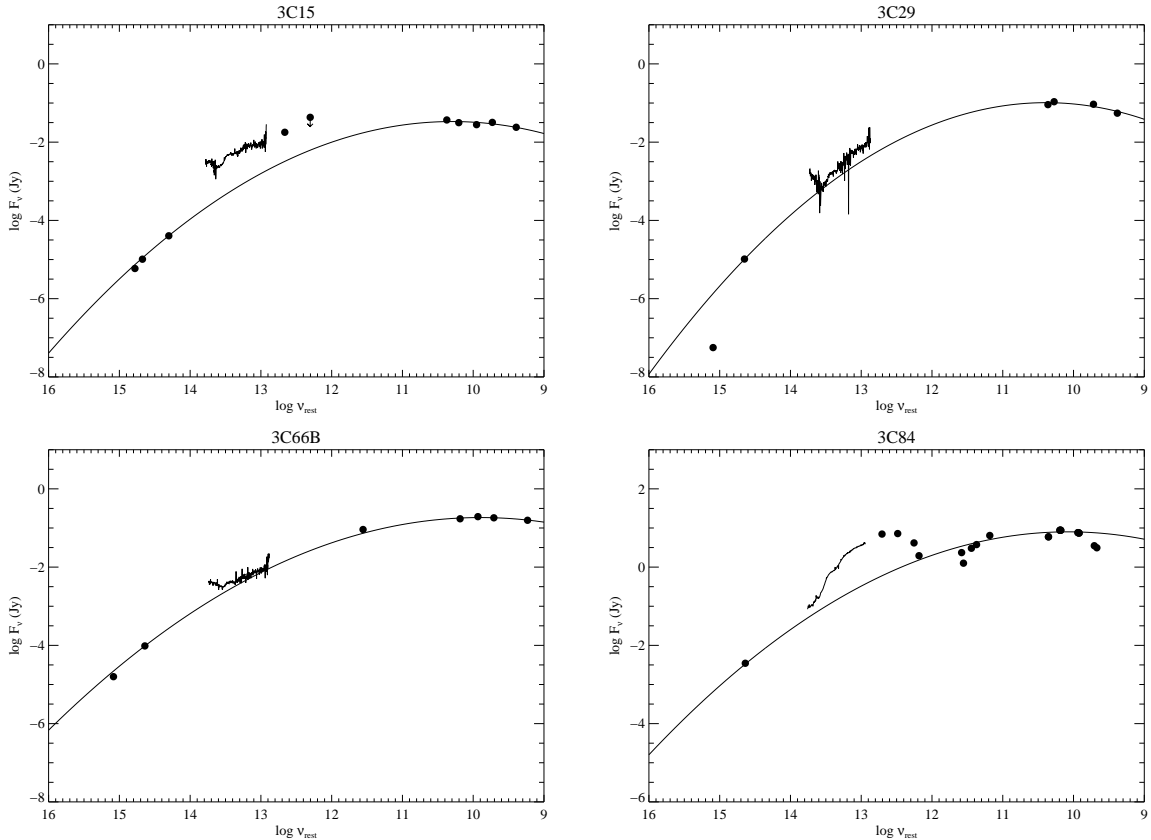


Fig. 7.— Observed nuclear SEDs for sources in which significant residual continuum emission could be identified. We used optical fluxes (Tab. 1), corrected for galactic absorption, nuclear NIR fluxes, and radio core flux measurements (arcsecond and sub-arcsecond scales). Only optical/NIR and radio core measurements were used for the parabolic fits. Nuclear UV (Chiaberge et al. 2002) fluxes, also corrected for galactic absorption, MIR/FIR, and sub-millimeter data (if available) as well as MIR spectra (this work) are overplotted. For sources with significant PAH features we have subtracted the star formation component (3C84, 3C270, IC4296, NGC 6251; see text).

flux, B is the log of the peak frequency of the parabola, and A represents a “curvature” parameter). We note that a similar parabolic function can also be used to describe the SEDs of BL Lacs in $\log \nu F_\nu$ vs. $\log \nu$ (e.g. Nieppola et al. 2006).

In order to construct the (nuclear) SEDs, photometric data from the literature have been compiled from optical through radio wavelengths. For the radio and optical we only focused on core emission and we only compiled these data for sources with detected optical CCC components. In total our sample has 14 objects in common with the sample of Chiaberge et al. (1999). But for two sources no CCCs could be identified: for 3C293

Chiaberge et al. (1999) could not estimate any CCC flux due to large scale dust structures in the host galaxy, and 3C424 showed a “radically different” nuclear behavior (i.e., the FWHM of the nuclear source is much larger than for other CCCs and it is spatially resolved). This leaves 12 sources. In following works CCCs were also detected in 3C15 (R. Baldi as well as M. Chiaberge, private communication), in 3C189 (Capetti et al. 2002), in IC4296 (Balmaverde et al. 2006a), and in NGC 6251 (Chiaberge et al. 2003). Thus, 16 sources here have an optical CCC detected (Tab. 1). Compared to other CCC objects, 3C386 stands out in the properties of its optical CCC

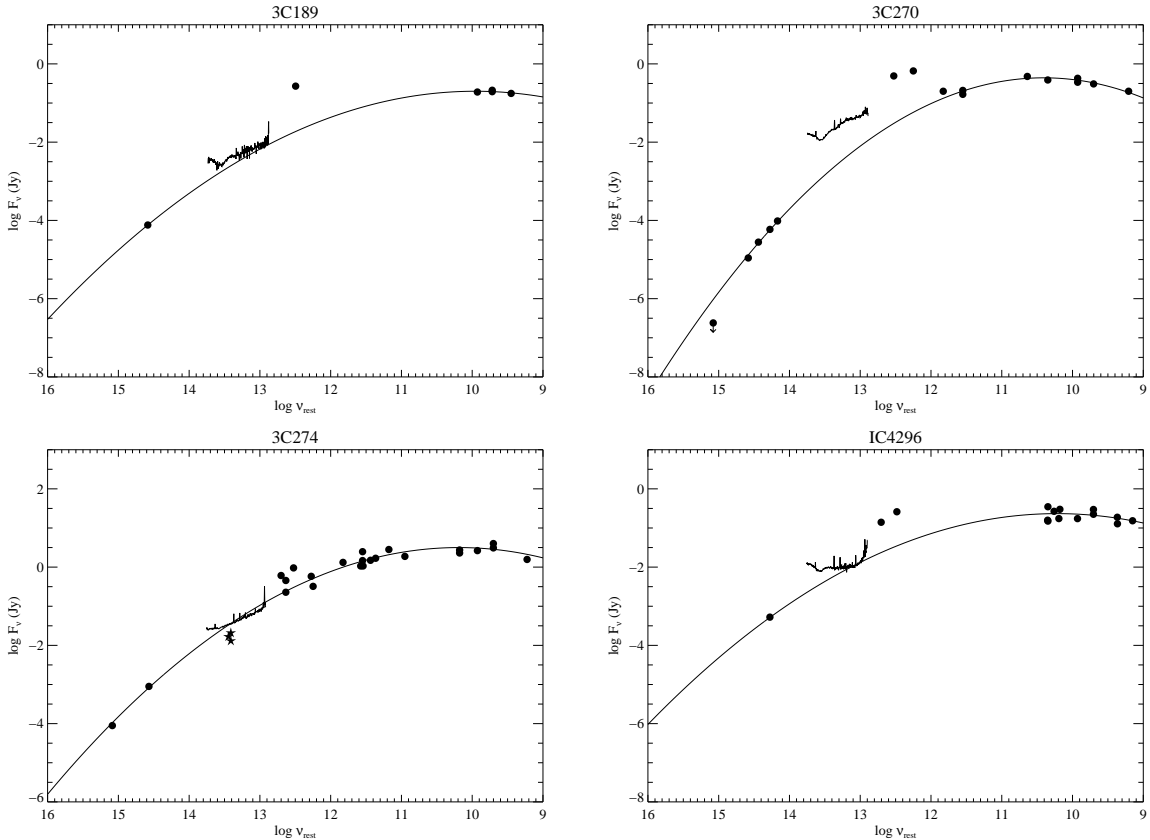


Fig. 7.— *continued.*

which is exceptionally bright compared to the radio core. It has been suggested (Chiaberge et al. 1999), supported by the tentative detection of a broad optical emission line (Simpson et al. 1996) that this source shows additional optical flux from a Big Blue Bump component, i.e. showing the central core of a type-1 AGN. However, it seems more likely that the foreground star which falls right on top of the nucleus (Lynds 1971; Madrid et al. 2006; Buttiglione et al. 2009) mimics an optical CCC because we do not see any signs for such a type-1 AGN in the MIR. In fact, after subtracting some emission due to star formation the residual spectrum can be explained well by a quiescent early-type galaxy (Fig. 13). In addition, new optical spectroscopy does not confirm a broad H α emission-line component (Buttiglione et al. 2009). Because we cannot tell whether or not 3C386 itself shows a compact optical core we here exclude this object from further analysis. This leaves 15

sources where optical CCCs are securely detected. Eleven of the 15 objects also show residual MIR emission⁵, while the spectra of four sources are dominated by processes from the host galaxy (stellar emission, star formation).

We used the parabolic function to fit only the radio core data and the optical CCCs which are both claimed to be synchrotron emission from the same source (e.g. Chiaberge et al. 1999; Hardcastle & Worrall 2000). For these data we know that they are nuclear and fairly robust while other measurements might still be affected by either intrinsic absorption (UV) or aperture effects (MIR, FIR, sub-mm)⁶.

⁵Recall that if our methodology is correct the presence of residual emission means they contain AGN heated dust and/or prominent synchrotron contributions, i.e. a nuclear source of MIR continuum emission.

⁶Because the core flux data were compiled from the literature they are generally not obtained simultaneously which

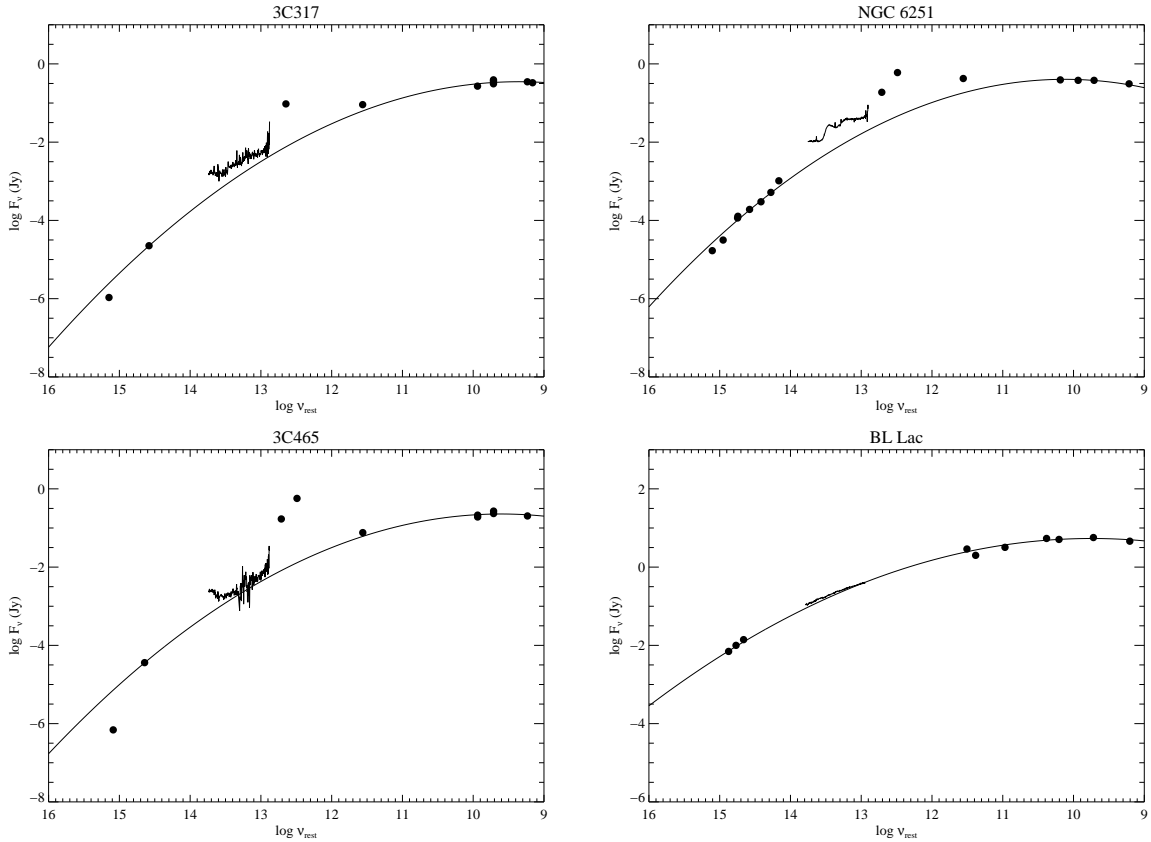


Fig. 7.— *continued.*

4.4.1. Sources with residual MIR emission

In the following we will discuss the SEDs on an object to object basis. References to flux measurements used for the SED plots (Fig. 7) in addition to those already given in Tab. 1 are also noted. In Tables 2 and 3 we give the percentage contributions of the estimated non-thermal component to the observed MIR flux.

3C15 This source shows MIR continuum emission which is not due to either star formation or stellar emission (Fig. 3). Using optical and NIR CCC measurements (provided by R. Baldi as well as M. Chiaberge, private communication) and radio core data the non-thermal core component clearly underestimates the observed MIR flux.

can result in variability becoming important for the quality of the fits. However, in most cases all the multi-epoch data can be fitted well and any scatter present due to intrinsic variability seems relatively small.

However, we point out that 3C15 has a strong arcsecond-scale jet (Leahy et al. 1997) which is also detected in the optical (Martel et al. 1998) and in X-rays (Kataoka et al. 2003). Since the extended jet is included in both IRS slits (SL slit oriented along the jet axis, LL slit oriented perpendicular to the jet axis) it can potentially make additional non-thermal contributions to the MIR spectrum. The inspection of the 2-D spectral images from IRS does not reveal any secondary component in the SL profile but the spectrum appears dominated by a single source (the size of the jet is almost comparable to the resolution of *Spitzer* at IRS wavelengths).

At 8.4 GHz the total radio flux of the arcsecond jet is greater than the core flux by a factor of ~ 10 (Leahy et al. 1997; Hardcastle et al. 1998). Assuming a typical jet spectral index of $\alpha \sim -0.6$ (Bridle & Perley 1984) this would lead to a non-thermal jet contribution of 2 mJy and 3 mJy at

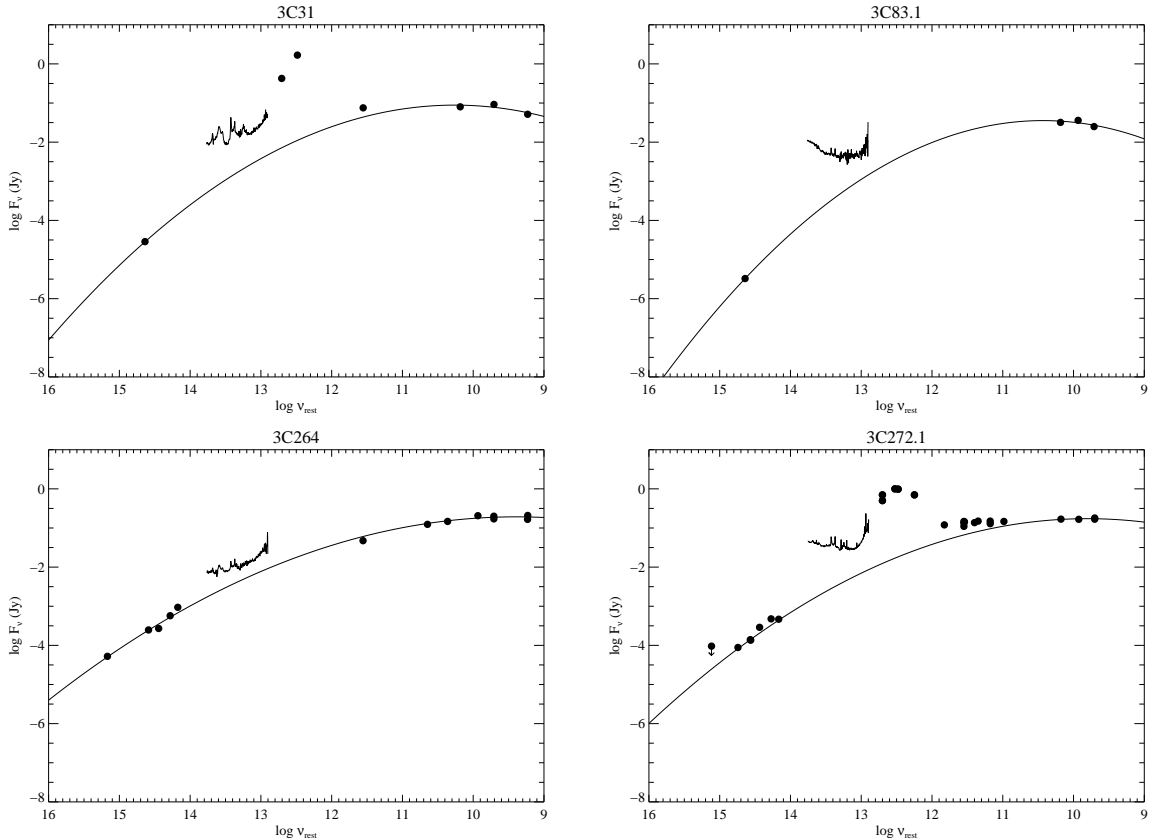


Fig. 8.— Same as in Fig. 7 but for sources which are dominated by processes in the host galaxy (star formation and/or stellar emission). Here, we show the observed MIR spectra.

$15\ \mu\text{m}$ and $30\ \mu\text{m}$, respectively, in the case of a single power law. For this conservative estimate we used a spectral index which is quite flat for a jet. In fact, the radio–optical spectral index of the X–ray brightest jet knot (“Knot C”, Kataoka et al. 2003) is argued to be steeper than our chosen value (Kataoka et al. 2003; Dulwich et al. 2007).

Thus, even under the assumption of a conservatively flat spectral index for the jet the total non–thermal contribution (core + jet) to the MIR emission within the IRS apertures is still a factor of ≥ 2 smaller than the total observed emission. In addition, the spectrum itself shows a change in slope around $\sim 20\ \mu\text{m}$ (which could be identified with a $18\ \mu\text{m}$ silicate feature) which argues for thermal contributions to the total flux.

Considering the appearance of the spectrum (including the potential $18\ \mu\text{m}$ silicate feature), the absence of notable PAH emission, and the dif-

ference between total flux and (conservatively estimated) non–thermal contributions we therefore argue that 3C15 shows thermal MIR emission from warm nuclear dust, possibly heated by an AGN.

We also note that Rinn et al. (2005) observe the X–ray core of 3C15 to be fairly weak ($L_{2-10\ \text{keV}} \sim 5 \times 10^{40}\ \text{erg/s}$ intrinsic) but absorbed by a significant column density of $N_{\text{H}} \sim 9 \times 10^{22}\ \text{cm}^{-2}$. *References:* Dicken et al. (2008); Hardcastle et al. (1998); Morganti et al. (1997)

3C29 The parabolic fit matches the radio data quite well but greatly overpredicts the nuclear UV measurement. Assuming that this is due to extinction, dereddening of the UV flux in order to match it with the synchrotron fit would also result in increasing the optical flux somewhat. Such a synchrotron SED could in principle account for the small excess in the MIR spectrum. In fact, Chiaberge et al. (2002) note that the UV

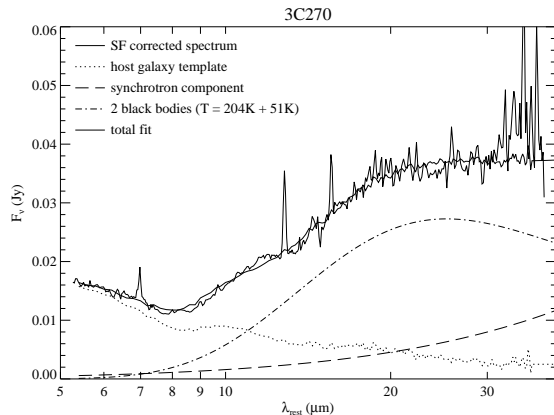


Fig. 9.— The star-formation corrected spectrum of 3C270 is fitted with the spectrum of the elliptical galaxy NGC 1549 (dotted line), the synchrotron component from the core (dashed line), and two black bodies (dot-dashed line; see text for details).

point in 3C29 might be absorbed by a thin, extended dust lane. However, the mismatch of the UV measurement could also arise from variability. While the optical and UV data were obtained more than 5 years apart, the difference between the synchrotron estimate and the actual UV measurement corresponds to a factor of ~ 30 in flux. This seems high to be solely due to variability. Considering that some absorption in the UV/optical bands is present, that the slope of the MIR spectrum agrees reasonably well with the synchrotron fit, and that no host corrections were applied the MIR emission in this source is likely to be mostly non-thermal. *References:* Morganti et al. (1997); Ricci et al. (2006)

3C66B Here all data points (including the UV and MIR) agree very well with the parabolic fit. Thus, there does not seem to be significant extinction present in this object and the residual MIR emission is very likely to be non-thermal. At the shortest wavelengths of the MIR spectrum the stellar population of the host galaxy can be seen. 3C66B has an arcsecond-scale jet (Hardcastle et al. 1996) which is also seen in the optical (Butcher et al. 1980; Macchetto et al. 1991; Perlman et al. 2006), in X-rays (Hardcastle et al. 2001), and even at MIR wavelengths a detection with *ISO* is claimed

(Tansley et al. 2000). However, unlike the case of 3C15, the jet in 3C66B is weaker than the core. Hardcastle et al. (2001) fit the radio through X-ray jet spectrum with a broken power-law model where the steepening from $\alpha \sim -0.5$ to $\alpha \sim -1.35$ occurs in the infrared. The radio-IR spectral slope agrees reasonably with the $14.5 \mu\text{m}$ MIR jet flux of $\sim 1.7 \text{ mJy}$ estimated by Tansley et al. (2000). Considering these values the jet contribution in the MIR is only $< 50\%$ of that of the core. Thus, the inclusion of the jet in the IRS spectral aperture does not alter our conclusion for the dominance of non-thermal MIR emission in nucleus of 3C66B. *References:* Jackson et al. (1993); Xu et al. (2000); Quillen et al. (2003); Kharb et al. (2005)

3C84 While this source is strongly core dominated in the radio, a clear dust emission bump is observed which reaches from the FIR well into the MIR. The SED is very complex and suffers from resolution effects (sub-mm vs. VLA vs. VLBA), which reduce the quality of the synchrotron core fit. In addition the VLBA data suggest self absorption in the core making the SED asymmetric which cannot be fitted well with a parabolic function. Therefore, the fit was limited to the optical core and the radio core measurements excluding the 5 GHz data where the downturn in the SED is already quite prominent. Besides the resolution effects and the self absorbed core, variability might also be important and the fit cannot be more than a rough approximation of the synchrotron core component in this case. However, the thermal MIR and FIR bump is very pronounced in 3C84 and variations in the underlying synchrotron component are almost negligible at these wavelengths.

The MIR spectrum itself does not show significant contribution from stellar emission, only minor indications for star formation, and overall has a spectral appearance quite similar to “thermal” spectra of AGN powered sources. The fact that the spectrum is on average almost an order of magnitude brighter than the underlying non-thermal core emission strengthens the argument for thermal dust emission in 3C84, powered by a central engine. In addition, Ho et al. (1997b) find broad emission-line components in $H\alpha$ and other permitted lines. *References:* Knapp & Patten (1991); Quillen et al. (2003); Haas et al. (2004); Stickel et al. (2004); Taylor et al. (2006)

3C189 In the observed MIR spectrum this source is very similar to 3C66B (Fig. 1). Also in the context of the SED we see that the fit to the synchrotron core matches with the MIR emission in shape as well as in flux. An *IRAS* 100 μm flux measurement indicates the presence of cool (possibly extended) dust. *References:* Bridle & Fomalont (1978); Knapp et al. (1990); Giovannini et al. (1994)

3C270 Including nuclear NIR measurements as well as (large aperture) FIR and (sub)–mm data, the SED has very good coverage. We see that the radio core data, the NIR, and the (sub)–mm data fit well with the synchrotron prediction, arguing for their common non–thermal origin. The MIR spectrum, however, shows a very clear excess over the underlying non–thermal emission. Not only does the excess in MIR flux indicate additional thermal emission from warm dust in this source, but also the shape of the *Spitzer* spectrum makes its nature as non–thermal emission very unlikely. The pronounced change of slope around $\lambda \sim 20 \mu\text{m}$ rest wavelength (Fig. 5) strongly suggest thermal emission from warm dust to be present in this source.

In fact, after subtracting the star–forming template from the spectrum the MIR continuum can be well fitted as a combination of the underlying synchrotron contribution and the elliptical template for the host galaxy, plus a black body with a temperature of $\sim 200 \text{ K}$ (Fig. 9)⁷. This emission from warm dust is not powered by star formation because this would result in accompanying PAHs. At 15 μm the continuum emission of this residual thermal MIR component has a luminosity of $\nu L_{\nu, 15 \mu\text{m}} \sim 4 \times 10^{41} \text{ erg s}^{-1}$ (see also Tab. 3).

In the optical, Barth et al. (1999) report a broad $\text{H}\alpha$ line in polarized light. This (tentative) detection further supports the presence of a classical hidden AGN. Moreover, a geometrically thick

⁷The fit to the star–formation corrected spectrum has only 3 variable parameters: the scaling of the elliptical template as well as the temperature of the two black bodies. Because the synchrotron component was determined independently from radio/optical core measurements its flux was held fixed. We note that the colder black body is not well constrained but including it improves the fit for $\lambda > 20 \mu\text{m}$. However, the presence or absence of this second black body leaves the temperature of the warmer component virtually unchanged as it is strongly constrained by the continuum between 10 and 20 μm .

nuclear dust disc has been observed in silhouette (Jaffe et al. 1993). We also note that the optical emission–lines in the nuclear region have flux ratios expected for Seyferts (Ferrarese et al. 1996; see §4.8).

Several studies are in broad agreement on the basic X–ray properties like the moderate intrinsic luminosity of $L_{2-10 \text{ keV}} \sim 1 \times 10^{41} \text{ erg/s}$ and the moderate absorption on the order of $N_{\text{H}} \sim 5 \times 10^{22} \text{ cm}^{-2}$ (Chiaberge et al. 2003; Gliozzi et al. 2003; Sambruna et al. 2003; Rinn et al. 2005; Zezas et al. 2005). The origin of the observed X–ray emission is, however, controversially discussed: While Chiaberge et al. (2003) interpret the X–ray power–law component as due to the jet, Gliozzi et al. (2003) argue in favor of an accretion flow as the most likely source for the bulk of the X–ray emission. On the other hand, Zezas et al. (2005) state that both processes are able to explain the observed X–ray properties. A Fe K α line is (marginally) detected with an equivalent width of $\sim 230 \text{ eV}$ (Gliozzi et al. 2003; Sambruna et al. 2003; Rinn et al. 2005) which is consistent with the upper limits from other studies (e.g. Chiaberge et al. 2003; Zezas et al. 2005).

While the warm dust might represent the same nuclear absorbing material detected in X–rays we note that due to the large *Spitzer* slit width our spectra include the prominent $\sim 300 \text{ pc}$ nuclear dust disc. In principle the 200 K dust observed in the MIR could correspond to this dust disc. Because in situ star formation as a heating mechanism can be largely excluded (no PAHs) another source of sufficient energy needs to be present in the nucleus of 3C270. Radiation from a (possibly hidden) active nucleus is an obvious possibility. However, in the case of heating by the low–to–medium luminosity AGN in 3C270 simple energy budget arguments strongly suggest the $\sim 200 \text{ K}$ dust to reside on much smaller scales than $\sim 300 \text{ pc}$. *References:* Jones & Wehrle (1997); Capetti et al. (2000); Jones et al. (2000); Quillen et al. (2003); Haas et al. (2004); Kharb et al. (2005)

3C274 Interestingly, the slope of the *Spitzer* spectrum appears flatter than what one would expect according to the synchrotron core fit. After accounting for host galaxy light using the elliptical template the MIR continuum alone can be well fitted with a single power law of $\alpha \sim -0.80$

for wavelengths shorter than $\sim 25 \mu\text{m}$. At longer wavelengths the spectral slope steepens with respect to the power law which might be due to an additional dust component (Perlman et al. 2007). As discovered by Whysong & Antonucci (2001) and later discussed by Perlman et al. (2001) and Whysong & Antonucci (2004), an unresolved $\sim 0.5''$ MIR core is present in 3C274. The MIR spectrum is discussed in detail by Perlman et al. (2007). *References:* Knapp & Patten (1991); Xu et al. (2000); Nagar et al. (2001); Quillen et al. (2003); Haas et al. (2004); Lister & Homan (2005); Perlman et al. (2001, 2007); Shi et al. (2007a); Whysong & Antonucci (2004)

IC4296 For IC4296 the synchrotron fit falls very close to the MIR spectrum, but only for a very narrow wavelength interval ($\lambda \sim 20 - 30 \mu\text{m}$). In this source a star-forming template has been subtracted because PAHs are clearly detected and the spectrum seems to be dominated by stellar emission shortwards of $\lambda \sim 10 \mu\text{m}$ (Fig. 14). Above $25 \mu\text{m}$ a considerable steepening is observed in the spectrum suggesting the presence of a thermal bump in the SED due to cooler dust which is supported by FIR measurements. Despite the influence of processes in the host galaxy at some IRS wavelengths, this source has a very strong non-thermal contribution of greater than $> 60\%$ at $15 \mu\text{m}$ and $30 \mu\text{m}$ (Tab. 2). Although the synchrotron signature is weaker than for sources like 3C66B or 3C189 it manifests as clear residual MIR emission. Interestingly, Pellegrini et al. (2003) argue that the X-ray core in IC4296 ($L_{2-10 \text{ keV}} \sim 1.6 \times 10^{41} \text{ erg/s}$ intrinsic) originates from the jet and the X-rays are observed to be only mildly absorbed ($N_{\text{H}} \sim 1 \times 10^{22} \text{ cm}^{-2}$). *References:* Killeen et al. (1986); Knapp et al. (1989); Morganti et al. (1997); Venturi et al. (2000); Pellegrini et al. (2003); Ricci et al. (2006)

3C317 For this source the MIR spectrum falls very close to the synchrotron fit in flux. The synchrotron curve overestimates the nuclear UV measurement somewhat and a similar situation of absorption intrinsic to the source or variability as in 3C29 could be imagined. In fact, Chiaberge et al. (2002) reported a factor of ~ 10 in variability for the nuclear UV point source. Thus, the discrepancy of the CCC measurements (and the offset in MIR flux) is likely to be caused by variability. The similarity in spectral shape and

the reasonable match in flux (combined with the absence of star-formation tracers) strongly suggest the dominance of non-thermal emission in the MIR. *Spitzer* FIR measurements at $70 \mu\text{m}$ suggest the presence of cold dust in this object. *References:* Zhao et al. (1993); Venturi et al. (2000); Quillen et al. (2003, 2008)

NGC 6251 Using UV, optical, and NIR measurements (Chiaberge et al. 2003) and multi-frequency radio core measurements (VLBI, Evans et al. 2005b), a well sampled nuclear SED can be constructed for NGC 6251. As for other sources, variability might be an issue for the non-thermal core measurements and in fact variability with a factor of ~ 2 over a few years has been reported for the nuclear (VLBI) radio component (Evans et al. 2005b). However, the radio measurements shown here were obtained simultaneously and the fit also agrees well with most of the multi-epoch *HST* measurements. For this source the MIR spectrum shows a clear excess over the synchrotron core fit, even after the correction for some minor star formation as traced by PAH emission of small equivalent width (Fig. 1). The small contribution from star formation, the absence of signs for significant contributions from stellar emission, and the overall shape of the spectrum (including the strong silicate emission features) strongly suggests a considerable component of thermal MIR emission in the nuclear regions of NGC 6251. The spectrum also looks quite different from other sources which are dominated by non-thermal emission in the MIR (e.g. 3C66B, 3C189 in Fig. 7).

At $30 \mu\text{m}$, where the strong silicate emission features will have only a minor impact on the continuum luminosity (e.g. Spoon et al. 2007), we measure $\nu L_{\nu} = 5.6 \times 10^{42} \text{ erg s}^{-1}$ in the spectrum. On the other hand, the luminosity of the synchrotron component at this wavelengths is about $\nu L_{\nu} \sim 2.2 \times 10^{42} \text{ erg s}^{-1}$, which is consistent with the $\nu L_{\nu} \sim 2.5 \times 10^{42} \text{ erg s}^{-1}$ given by the synchrotron self-Compton SED fit of Chiaberge et al. (2003). We note however, that the factor of ~ 2.5 luminosity difference between the synchrotron core and the MIR spectrum is of the order of the measured radio core variability. In principle, the excess of the spectrum could be accounted for by variability of the underlying synchrotron core component. Although this would change the thermal to non-thermal ratio in the MIR (with the

Table 2: Estimated contributions to the MIR spectra for sources without detected AGN dust components.

Object	$F_{15\mu\text{m}}$ (rest frame)				$F_{30\mu\text{m}}$ (rest frame)				comment
	total ^a mJy	SF %	stars %	synch ^b %	total ^a mJy	SF %	stars %	synch ^b %	
sources without optical core measurements									
3C76.1	1.72	21	0	...	3.53	30	0	...	low S/N spectrum
3C129	3.26	17	46	...	11.44	14	6	...	
3C218	4.49	100	0	...	15.91	100	0	...	SF dominated spectrum
3C293	20.10	100	0	...	57.98	100	0	...	SF dominated spectrum
3C386	1.97	16	74	...	1.78	52	37	...	foreground star mimics CCC
3C403.1	< 1.34	< 1.53	not detected
3C424	1.52	...	12	...	5.06	...	2	...	
sources with optical core measurements									
3C29	2.48	...	15	58	8.16	...	2	42	peak-up spill-over ^c , UV abs.
3C31	13.99	87	0	13	29.30	86	0	14	SF dominated spectrum
3C66B	4.76	...	21	79	8.72	...	5	85	
3C83.1	4.08	18	64	12	5.37	40	22	22	low PAH ratio
3C189	4.80	...	20	71	8.73	...	5	79	cold dust
3C264	9.11	52	0	48	23.88	67	0	33	SF dominated spectrum
3C272.1	28.08	30	57	13	46.70	53	15	15	cold dust, low PAH ratio
3C274	43.25	...	7	93	81.38	...	2	98	
IC 4296	10.02	6	30	69	19.88	9	7	68	cold dust
3C317	2.90	...	16	50	5.86	...	3	57	
3C465	3.08	...	19	68	7.47	...	3	59	cold dust
BL Lac	246.45	...	0	100	381.92	...	0	100	

^aFlux measured from the observed MIR spectrum.

^bFlux of the synchrotron component shown in Figs. 7 and 8.

^cDue to the peak-up spill-over the spectral slope and flux at short wavelengths might be compromised. This adds some uncertainty to the scaling of the stellar template.

NOTE.—The contributions of the individual components do not necessarily add up to 100%. This is due to the nature of our approach which uses fixed templates in a step-by-step manner in order to identify and correct successively for their contributions to the observed spectra. This naturally leaves room for variations between individual objects which can manifest as residuals or slight overcorrections. Also, components not considered might have an effect (e.g. cold dust, particularly at $30\mu\text{m}$). In addition, for sources with significant contributions from non-thermal emission variations in the nuclear components and obscuration for UV/optical data might result in some mismatch and residual emission. See text for comments on individual sources where this might be the case.

non-thermal part potentially even dominating at times) the appearance of the MIR spectrum still argues for the existence of warm nuclear dust in NGC 6251.

Ferrarese & Ford (1999) report the tentative detection of a broad component in H α (this result seems to be strongly dependent on the assumed modelling of the narrow lines though). In X-rays the power-law component in NGC 6251 shows only very little absorption ($N_{\text{H}} \sim 5 \times 10^{20} \text{ cm}^{-2}$) and has an intrinsic lumi-

nosity of $L_{2-10 \text{ keV}} \sim 4.8 \times 10^{42} \text{ erg/s}$ (Gliozzi et al. 2004; Evans et al. 2005b). The additional detection of a broad Fe K α line (EW $\sim 220 \text{ eV}$ and FWHM $\sim 0.6 \text{ keV}$) led Gliozzi et al. (2004) to argue in favor of the presence of a standard accretion disk. In their study the base of the jet is ruled out as the sole origin of the nuclear X-ray emission. Evans et al. (2005b) on the other hand question the significance of the K α detection and favor the jet as the source for the bulk of the observed X-ray core emission. However, they do not exclude

some contributions from an accretion flow. *References:* Golombek et al. (1988); Chiaberge et al. (2003); Quillen et al. (2003); Evans et al. (2005b)

3C465 The observed spectrum falls very close to the synchrotron core fit. Assuming that the observed nuclear UV component is also non-thermal, significant absorption seems to be present in this source. Alternatively, variability of a factor of ~ 10 could cause this UV flux difference. As noted before, both processes can in principle account for the remaining offset between the MIR spectrum and the synchrotron fit. A steepening of the spectrum is observed for wavelengths larger than $\sim 30 \mu\text{m}$ indicating a thermal bump at FIR wavelengths. This is supported by *IRAS* 60 and $100 \mu\text{m}$ fluxes. *References:* Golombek et al. (1988); Venturi et al. (1995); Quillen et al. (2003); Jetha et al. (2006)

BL Lac Using quasi-simultaneous flux measurements from Landau et al. (1983) we construct an SED of this object, which is here used as an example for a strongly aligned, highly beamed FR-I source. Note that although no *HST* data were used the (ground-based) optical fluxes will be dominated by the core emission. The measurements can be well fit by the parabolic function and even though the MIR spectrum was obtained at a different epoch, it fits extremely well with the estimate for the synchrotron core emission. The spectrum can be fitted with a power law with $\alpha \sim -0.7$.

References: Landau et al. (1983)

4.4.2. Sources without residual MIR emission

In the following we will present the sources with detected CCCs but where no significant residual MIR continuum emission can be identified. The observed spectra can be explained by star formation and/or stellar emission. The SED plots are shown in Fig. 8.

3C31 This source is strongly dominated by star formation in the host galaxy (Fig. 1). Its observed spectrum is almost an order of magnitude brighter than then underlying non-thermal component. Interestingly, the SL aperture for the MIR spectrum is roughly consistent with the size of the molecular disk observed in the center of this source (Okuda et al. 2005). *IRAS* 60 μm and $100 \mu\text{m}$ measurements indicate substantial amounts of colder FIR dust. *References:* Burch

(1977); Xu et al. (2000); Evans et al. (2005a)

3C83.1 The few existing data points for the core emission are well approximated by the parabolic fit. The total light spectrum is dominated by processes in the host galaxy and lies well above the synchrotron fit. The subtraction of the star-forming template leaves a negative residual at the location of the $7.7 \mu\text{m}$ PAH feature (Fig. 6). As discussed above, this cannot be accounted for by the stellar spectrum of the host galaxy and argues for a low $7.7 \mu\text{m}$ to $11.3 \mu\text{m}$ PAH ratio which might in fact be powered by low-luminosity AGN activity instead of star formation (see §4.1). *References:* O’Dea & Owen (1986); Xu et al. (1999)

3C264 While the observed spectrum of this source is dominated by star formation, it falls much closer to the synchrotron component than in 3C31. From Fig. 8 we see that the non-thermal contribution might not be negligible (see also Tab. 2). However, without prior knowledge of this fact the source spectrum can be fitted by star formation only due to the wide variety in the MIR spectral properties of star-forming galaxies (e.g. Dale et al. 2005; Brandl et al. 2006; Smith et al. 2007).

We note that this source has an arcsecond-scale radio jet (e.g. Lara et al. 2004) which is also detected at optical wavelengths (Crane et al. 1993; Baum et al. 1997). However, in the radio the core is stronger than the total jet emission and has a significantly flatter spectrum (Lara et al. 2004). While the jet emission steepens even more at optical wavelengths the contributions in the MIR are negligible compared to the core. *References:* Xu et al. (2000); Lara et al. (2004); Kharb et al. (2005)

3C272.1 The unusual sharp turn from a slightly blue slope into a steep, red slope observed in the MIR spectrum of this source is supported in the framework of the SED where several FIR measurements indicate the presence of a strong thermal bump from cool dust. The spectrum lies well above the core synchrotron fit at almost all wavelengths and comes closest near $\lambda \sim 25 \mu\text{m}$ where the slope change takes place (Fig. 6). The combination of strong PAH emission and a very low PAH $7.7 \mu\text{m}$ to $11.3 \mu\text{m}$ ratio results in a prominent depression at the location of the $7.7 \mu\text{m}$ feature after subtraction of the star forming template. As discussed above (§4.1) the unusual

Table 3: Estimated contributions to the MIR spectra for sources with detected AGN dust components (see notes to Tab. 2).

Object	F _{15 μm} (rest frame)					F _{30 μm} (rest frame)					comment
	total mJy	SF %	stars %	synch %	AGN ^a %	total mJy	SF %	stars %	synch %	AGN ^a %	
3C15	5.52	...	19	14	67	9.15	...	5	18	77	peak-up spill-over ^b
3C84	1307.88	1	0	12	86	3859.70	1	0	9	90	
3C120	345.79	2	0	...	98	653.08	11	0	...	89	type-1 AGN
3C270	27.45	7	21	11	61	52.14	27	5	16	52	
NGC 6251	27.88	3	0	29	68	49.68	5	0	33	62	
E1821+643	333.78	2	0	...	98	540.74	9	0	...	91	type-1 AGN

^aThe contribution of the AGN component (which dominates in these objects) was determined as the total flux minus the other three contributions considered here.

^bSee comment on 3C29 in Tab. 2.

PAH ratio might point toward AGN excitation instead of star formation but we count this source here as host dominated. *References:* Bower et al. (2000); Leeuw et al. (2000); Nagar et al. (2001); Haas et al. (2004); Leeuw et al. (2004); Doi et al. (2005)

4.5. Sources without CCC measurements

In §4.4 we study the contributions of the synchrotron cores to the MIR emission in our sources. However, this test is limited to objects where optical CCC measurements are available. When using the CCC fluxes in combination with radio core data, a nuclear SED can be constructed which bridges the MIR wavelengths. This way a fairly robust estimate of the non-thermal component can be achieved which helps to distinguish between thermal and non-thermal contributions to any residual MIR emission (i.e. emission not resulting from star formation or stellar processes).

Where no CCC measurements are available, a reliable estimate of the synchrotron core contribution to the MIR emission is not possible. However, the overall shape of the spectrum might still provide indications on which process – thermal or non-thermal – dominates the MIR emission. Out of the 25 sources considered in this paper, 7 objects do not have CCC measurements available. We here briefly comment on these seven sources:

3C76.1 The MIR spectrum of this source can be well explained by a combination of star forma-

tion and stellar emission. No significant residual continuum can be identified. However, this spectrum suffers from low S/N which limits the reliability of any conclusions regarding the MIR continuum constituents.

3C129 After correcting for some contributions from star formation and accounting for stellar emission from the host galaxy, 3C129 shows strong, red continuum emission longwards of $\sim 15 \mu\text{m}$ (Fig. 13). Inspecting Fig. 13 reveals that we could in principle have used a star-formation template with a steeper MIR/FIR slope which would reduce the level of residual continuum. However, given the lack of any strong optical emission lines, the general appearance of the optical spectrum, and the clear dominance of an old stellar population (as determined by Buttiglione et al. 2009), it seems unlikely to us that this source harbors the stronger star formation which could power the redder MIR/FIR colors of a different template. However, while residual nuclear continuum emission is observed in 3C129 we cannot discriminate between a thermal or non-thermal origin because we lack optical CCC measurements. But we note that the residual MIR spectrum shows some concave upward curvature (Fig. 13) and is significantly different in appearance compared to objects like 3C66B or 3C189 in which the MIR continuum is dominated by non-thermal emission (Figs. 1,7). This argues in support of the thermal origin of the residual emission.

3C218 The MIR spectrum of Hydra A can

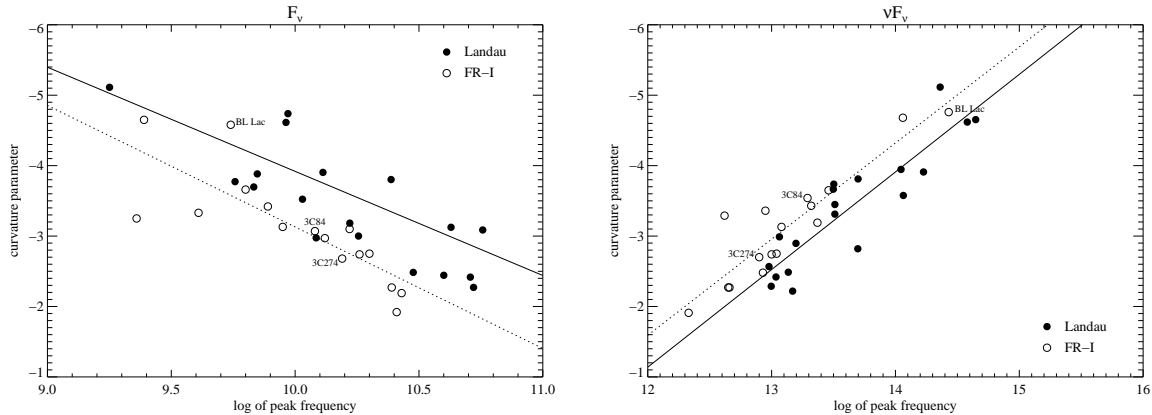


Fig. 10.— Curvature parameter plotted against the logarithm of the peak frequency for the core SED fits in F_ν (*left*) and νF_ν (*right*). Open symbols represent FR–I sources, filled symbols the blazars from Landau et al. (1986). The solid and dashed lines show linear least–square fits to the blazar and FR–I data points, respectively. Note that a smaller absolute number for the curvature parameter corresponds to a more strongly curved SED. We marked the sources BL Lac, 3C84, and 3C274 which are quite different from the lobe–dominated objects of our core sample but show extended radio emission of FR–I type.

be well explained by star formation only, perhaps with some minor contributions from stellar emission at the shortest MIR wavelengths (Fig. 2). Considering the equivalent width of the PAH features the continuum at $\lambda > 20 \mu\text{m}$ is in agreement with what can be expected for normal star forming galaxies. The presence of a very young stellar population is also seen in optical spectra (Melnick et al. 1997; Aretxaga et al. 2001; Wills et al. 2004).

3C293 The MIR spectrum of 3C293 is strongly dominated by star formation and no residual nuclear continuum can be identified (Fig. 1). In these properties it is quite similar to 3C31.

3C424 For 3C424 no significant contributions from star formation can be identified in the MIR spectrum and a weak and noisy, but securely detected, continuum can be seen.

3C120 and **E1821+640** are broad-line AGN, which have MIR spectra typical of their class, displaying strong silicate emission features and high ionization emission lines (Fig. 2).

4.6. Comparison with blazars and related objects

It has been suggested that most (but not all) FR–I radio sources are the misaligned coun-

terparts of BL Lac objects (Kollgaard et al. 1992; Urry & Padovani 1995; Cassaro et al. 1999; Antonucci 2002a). As outlined in §4.4, the SEDs of these strongly beamed, highly core dominated sources are well described by the same parabolic function we utilized to fit the cores of the FR–I objects (which is here used just as a fitting function for descriptive purposes).

In order to allow the comparison between the blazars and the FR–I cores we used the quasi–simultaneous data from Landau et al. (1986) to fit the blazars in the same way as the FR–Is. However, we limited the parabolic fit for the blazars to the radio (2 cm through 20 cm) plus optical R –band measurements, thus maximizing the comparability with the FR–I fits (the wavelengths of the nuclear FR–I data used to constrain their fits were very similar). Overplotting all the blazar data onto the fits obtained using only the limited data points shows that this approach yields a reasonable representation of the curved SEDs.

We will now compare the resulting fit parameters for peak frequency and SED curvature of the (putatively) misaligned sources with the respective data of their highly aligned (supposed) siblings. Moreover, we performed the SED fits not only in F_ν but also in νF_ν using the same parabolic function as given in equation (1) and using the

same set of nuclear data.

As already shown in e.g. Landau et al. (1986) a correlation of peak frequency and curvature in F_ν exists for blazars. For FR–I sources a very similar behavior is detected (Fig. 10). However, while both types of objects cover about the same range in F_ν peak frequencies there is a systematic offset for the FR–Is towards more strongly curved SEDs. A comparable result has been obtained using broad band spectral indices of FR–Is and low–energy peaked BL Lacs. These two types of objects overlap in their radio/optical power–law slopes but there is a clear tendency for FR–Is to have steeper α_{ro} than the BL Lacs (Hardcastle & Worrall 2000; Trussoni et al. 2003; Balmaverde et al. 2006a). Because for a parabola peaking at radio wavelengths (which is typically the case for the sources considered here) a steeper radio/optical single power–law slope corresponds to a higher curvature, our results shown in Fig. 10 are consistent with these previous findings.

In νF_ν the blazars also show a correlation between peak frequency and curvature, but now the FR–Is seem to continue this correlation at lower peak frequencies. However, we see no trend in the blazar distribution with FR morphology⁸. In particular, blazars with extended radio luminosities typical for FR–I objects do not necessarily concentrate towards the “classical” FR–I objects in Fig. 10, but seem to be randomly distributed within the blazar sample.

The lower peak frequency of FR–Is in νF_ν could be understood as a result of different beaming factors for the emission dominating in blazars and FR–I cores. This seems to be in agreement with the model of e.g. Chiaberge et al. (2000b) who assume that the jet has a velocity structure with a fast moving central spine (which is strongly beamed and dominates in aligned sources) and a slower – but still relativistic – outer layer of more isotropic, less strongly beamed emission which dominates in the misaligned cases. Due

⁸Using measurements for the extended radio luminosity associated with the blazars (Antonucci & Ulvestad 1985) we introduce a luminosity threshold (and varying this threshold between $\log L_{1.4 \text{ GHz, ext}}$ of 31.5 and 32.5 erg/s/Hz) for identifying “FR–I blazars”. Taking those blazars with extended radio luminosities below the threshold as the possible aligned counterparts for our misaligned FR–I sources we see no trend of blazar FR type in Fig. 10.

Table 4: 24 μm and [O III] emission–line fluxes.

Object	$F_{\text{rest}}(24 \mu\text{m})$ in mJy	$F([\text{O III}])$ in erg/s/cm ²	ref
3C15	8.63	3.15×10^{-15}	1
3C29	6.80	2.69×10^{-15}	1
3C31	19.16	4.71×10^{-15}	1
3C66B	7.42	1.10×10^{-14}	1
3C76.1	2.92	$< 2.91 \times 10^{-15}$	1
3C83.1	4.46	$< 1.85 \times 10^{-15}$	1
3C84	3130.13	5.89×10^{-13}	1
3C120	618.30	3.47×10^{-12}	7
3C129	6.95	$< 6.94 \times 10^{-15}$	1
3C189	7.57	2.05×10^{-15}	5
3C218	8.77	3.80×10^{-15}	8
3C264	15.05	1.47×10^{-15}	1
3C270	42.59	7.57×10^{-15}	2
3C272.1	29.52	5.11×10^{-15}	1
3C274	63.16	2.41×10^{-14}	1
IC4296	13.83	$< 1.74 \times 10^{-15}$	7
3C293	34.60	1.36×10^{-15}	1
3C317	4.74	8.32×10^{-15}	1
NGC 6251	41.98	5.20×10^{-15}	6
3C386	1.45	$< 2.53 \times 10^{-14}$	1
3C424	2.60	1.52×10^{-15}	1
3C465	5.12	3.11×10^{-15}	1
E1821+643	527.33	2.45×10^{-13}	3
BL Lac	332.69	3.82×10^{-15}	4

References. — (1) Buttiglione et al. 2009; (2) Ho et al. 1997a; (3) Kolman et al. 1991; (4) Lawrence et al. 1996; (5) SDSS; (6) Shuder & Osterbrock 1981; (7) Tadhunter et al. 1993; (8) Wills et al. 2004

to a shift in peak frequency of the emission, different amounts of relativistic beaming for aligned (i.e. BL Lac) and non–aligned (i.e. FR–I) sources would also affect the observed broad–band spectral indices. This can serve as one possible explanation for the difference in α_{ro} (or SED curvature) between FR–Is and BL Lacs (e.g. Chiaberge et al. 2000b; Trussoni et al. 2003; Balmaverde et al. 2006a).

4.7. MIR and emission–line luminosity

Under the assumption that the narrow–line region of AGN is extended and not affected by nuclear obscuration it has been argued that the

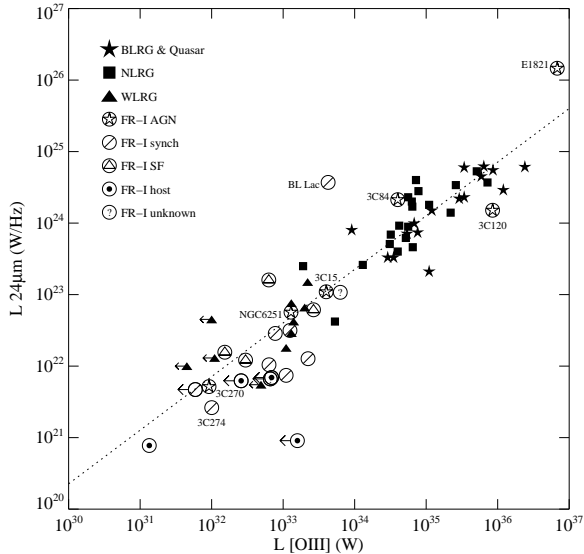


Fig. 11.— MIR luminosity at $24\ \mu\text{m}$ plotted versus the [O III] emission-line luminosity. We show the objects presented in Dicken et al. (2009) as filled symbols and the FR-I sources from this paper as open symbols. The FR-I points also indicate the dominating factor of the MIR emission: AGN – AGN-heated dust; synch – synchrotron emission; SF – star formation; host – stellar emission (plus possibly star formation). Sources labeled “unknown” (3C129 and 3C424) have MIR continuum emission in excess of host galaxy contributions but due to missing CCC measurements we cannot securely distinguish between AGN or synchrotron emission. The dashed line is the bisector of a linear least square fit to the filled symbols (see text for details).

luminosity of the [O III] $\lambda 5007\ \text{\AA}$ emission line can serve as an isotropic tracer of the intrinsic radiative AGN luminosity (Rawlings & Saunders 1991; Tadhunter et al. 1998). It has also been shown that for luminous AGN the radiative power, as traced by [O III], is correlated with the MIR luminosity at $24\ \mu\text{m}$ (Tadhunter et al. 2007; Dicken et al. 2009)⁹.

⁹For distant FR-II radio galaxies and quasars an interesting thread in the literature offers good evidence for the anisotropy of [O III], which we do not pursue here since we concentrate on FR-I objects. But these interesting references are e.g. Jackson & Browne (1990), Hes et al. (1993),

In Fig. 11 we plot the luminosity at $24\ \mu\text{m}$ versus the luminosity in the [O III] emission-line for the objects presented in Dicken et al. (2009, filled symbols) and for our FR-I sources (open symbols). We also show as a dashed line the bisector of a linear least square fit to the filled symbols¹⁰. While the AGN FR-I sources on average fall close to the bisector the visual inspection of Fig. 11 also reveals that the bulk of the remaining FR-I sources tend to have lower $24\ \mu\text{m}$ luminosities. In fact, a Kolmogorov–Smirnov test of the displacement in $L_{24\ \mu\text{m}}$ from the fitted line gives only a $\sim 1\%$ chance that two samples drawn from the same parent population would show a difference as strong as we see for the D09 sample and the non-AGN FR-I sources¹¹. The FR-I AGN sources on the other hand are statistically consistent with being drawn from the same parent population as the D09 sample. We note that this comparison assumes that the $24\ \mu\text{m}$ flux is dominated by an AGN component. While this is a reasonable assumption for the majority of the sources in the D09 sample (which mainly consists of NLRGs and quasars) we have shown here that it is certainly not the case for the non-AGN FR-I sources. For the latter the bulk of the MIR emission can be accounted for by other processes (Tab. 2).

The differences between FR-I sources with and without warm dust can also be established by comparing their respective MIR-to-[O III] luminosity ratios: We find $\log[\nu L_\nu(24\ \mu\text{m})/L([\text{O III})]] = 2.74 \pm 0.06$ for the four AGN FR-I sources but only a ratio of 2.06 ± 0.20 for FR-I sources without clear signs for

di Serego Alighieri et al. (1997), Simpson (1998). See also Haas et al. (2005) for an infrared/optical comparison.

¹⁰The bisector was determined using only the filled symbols and following the same strategy as Dicken et al. (2009): Sources with upper limits on their [O III] emission were excluded as well as sources with clear starburst signatures in their optical spectra. For the rest of this section we refer to this sample of 33 objects as the “D09 sample”.

¹¹In order to match the selection criteria of those two samples we excluded FR-I sources with [O III] upper limits from the K-S statistics as well as sources which are dominated by star formation (plus BL Lac).

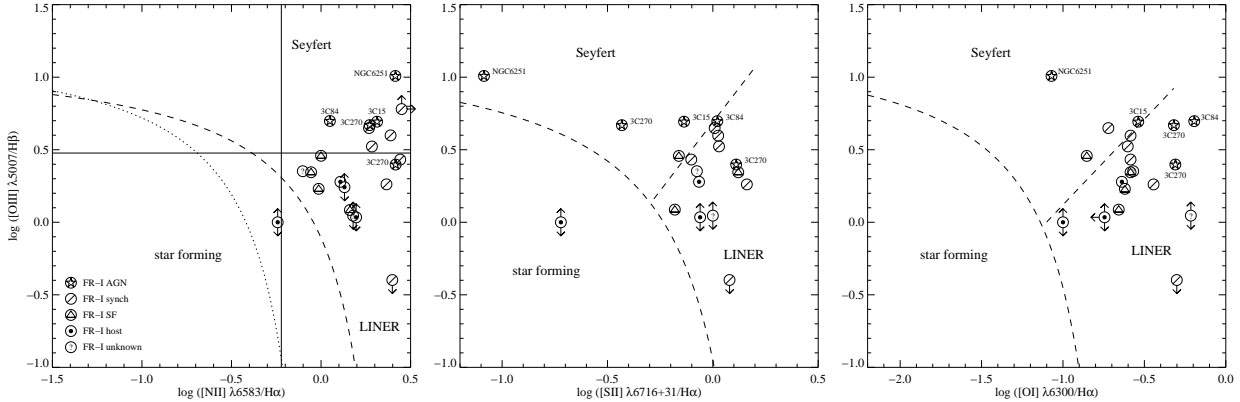


Fig. 12.— Diagnostic optical emission–line diagrams. On the left the dotted line is the dividing line used by Kauffmann et al. (2003) and the dashed line corresponds to the dividing line of Kewley et al. (2001). Sources with $[\text{N II}]/\text{H}\alpha > 0.6$ are often defined as Seyferts for $[\text{O III}]/\text{H}\beta > 3$ and as LINERs for $[\text{O III}]/\text{H}\beta < 3$. For the diagrams in the middle and on the right the dividing lines from Kewley et al. (2006) are used. The symbols are the same as in Fig. 11. For 3C270 the data point with the higher $[\text{O III}]/\text{H}\beta$ ratio corresponds to the small aperture *HST* data while the lower flux ratio represents the ground–based results (see text).

warm dust emission¹². The results of this exercise are just as we would expect from the spectral analysis and provide a strong consistency check for our method.

4.8. Diagnostic diagrams

Optical emission–line diagnostics are commonly used to identify the dominant activity type in line–emitting sources (e.g. Baldwin et al. 1981; Veilleux & Osterbrock 1987; Kewley et al. 2001; Kauffmann et al. 2003). Although we here largely focus on the MIR continuum properties of our FR–I sources, a brief study of their optical emission–lines ratios with respect to their MIR spectral “type” seems promising. We take data for the emission–line ratios either from the references given in Tab. 4 or from Hansen et al. (1995, 3C218) and from Lewis et al. (2003, IC4296).

In Fig. 12 we show three emission–line ratio diagrams for the FR–I objects (minus the broad–line sources 3C120 and E1821+643 and excluding BL Lac). Virtually all FR–Is, regardless of their

MIR properties, fall into the LINER or Seyfert region. Even the star–forming sources occupy the LINER region rather than showing HII–type emission–line ratios (this is discussed in the context of ULIRGs in e.g. Antonucci 2002a,b). Only one source (3C386) occupies the transition region (Fig. 12, *left*) or the HII region (Fig. 12, *middle*).

For the FR–Is with warm dust emission, 3C15 and NGC 6251 fall into the Seyfert region for all three diagrams, which historically requires the presence of an active nucleus in these objects. 3C84 and 3C270 on the other hand can be classified as Seyferts or as LINERs depending on which diagram is used (Fig. 12). This, however, also shows that sources which are LINERs optically can have significant emission from warm dust in the MIR. Interestingly, both of these LINERs with warm dust have broad emission–lines detected: 3C84 shows a broad $\text{H}\alpha$ component (Ho et al. 1997b) while Barth et al. (1999) report a (tentative) broad line in polarized light for 3C270. This is consistent with the findings of Sturm et al. (2006) who show that type–1 LINERs on average have an additional warm dust component compared to type–2 LINERs. Therefore we can speculate that LINERs with warm dust emission will also show broad emission lines.

Because nuclear emission–line ratios can be diluted by more extended emission from e.g. star

¹²We here exclude the luminous broad–line AGN 3C120 and E1821+643, the synchrotron dominated sources BL Lac and 3C274 as well as the four sources which are dominated by emission from star formation (Tab. 2). Note also that the slope of the fitted line shown in Fig. 11 is not equal one meaning that the $24\ \mu\text{m}/[\text{O III}]$ ratio changes with luminosity.

formation, especially for the weak and elusive sources considered here, we demonstrate the importance of aperture effects in the case of 3C270 which appears twice on each diagram: For every line–ratio combination shown (Fig. 12) 3C270 is always classified as a LINER when using the the emission–line fluxes measured in a $2'' \times 4''$ aperture (Ho et al. 1997a). However, considering only the line ratios for an *HST* spectrum of the very nuclear $0.09'' \times 0.09''$ (Ferrarese et al. 1996) places 3C270 in the Seyfert region for two out of the three diagrams.

Fig. 12 also reveals that some of the FR–Is which are dominated by synchrotron emission in the MIR (and which lack clear signs for substantial warm dust) exhibit Seyfert–like emission–line ratios and many fall very close to the LINER/Seyfert transition line.

5. Summary and conclusions

The MIR spectra of 25 FR–I radio galaxies are presented. Many of these sources show contributions from stellar emission at the shortest MIR wavelengths observed. The spectra generally turn over from a blue to a red continuum slope (in F_ν) around $\sim 10 \mu\text{m}$. Signs for star formation as traced by PAHs is detected in several objects and the relative contribution to the total spectra range from not detected (e.g. 3C66B, 3C317) to minor (e.g. 3C129, 3C270) to dominant (e.g. 3C31, 3C293).

Focusing on sources with detected optical compact cores, the nuclear SEDs for 15 objects are fitted with a parabolic function in order to estimate the synchrotron contribution to the MIR emission. For 7/15 objects (47%) the nuclear MIR emission turned out to be dominated by non–thermal processes: Apart from the stellar contributions at short wavelengths, the MIR spectra of these sources are consistent with the optical and radio core measurements. Mid–infrared continuum emission in excess over the synchrotron cores is detected in the 8/15 remaining sources. For four out of those eight objects the spectra are dominated by processes related to the host galaxy (star formation, stellar emission). The remaining four sources (27%) – 3C15, 3C84, 3C270, and NGC 6251 – show clear signatures of thermal MIR emission in excess over the non–thermal core contributions. This excess cannot be explained by either stellar

emission or star formation, which argues for the presence of thermal dust emission powered by an AGN. At least one of these objects has been (tentatively) confirmed to have a hidden type-1 AGN with spectropolarimetry.

Thus, for most of our sources in which the nuclear MIR component can be identified (and is not masked by host galaxy emission) this emission is likely to be of non–thermal origin. But some FR–I sources do exist which show evidence for a hidden AGN, consistent with findings at other wavelengths.

Parabolic functions were fitted to the radio and optical core data in order to estimate the nuclear synchrotron component. These fits were performed in F_ν as well as in νF_ν . Comparing the fit parameters for the FR–Is with those for a set of blazars and related objects, it appears that in F_ν both types of objects show a similar relation between the peak frequency and the curvature of the SED. However, while FR–Is cover about the same peak frequency range as the blazars used here for comparison, they show systematically stronger curvature in their SEDs. This reflects in the fit parameters for νF_ν where the FR–Is show on average smaller peak frequencies and again stronger SED curvature. Different amounts of relativistic beaming in BL Lacs and FR–Is could serve as a possible explanation for these results.

The comparison with a correlation between MIR and optical emission–line luminosity found for luminous AGN reveals that the AGN dominated FR–Is are consistent with that relation while the non–AGN FR–Is deviate substantially. In addition we show that FR–Is with and without warm dust differ significantly in their average $24 \mu\text{m}/[\text{O III}]$ luminosity ratio. The conclusion about the presence of an AGN in some of the FR–Is is further strengthened by their optical emission–line ratios. These tests provide a strong consistency check for our method.

One important conclusion of this paper, as well as of other results in the literature, is that while most FR–Is lack powerful type–1 AGN, it is not tenable to generalize on associations between FR–I galaxies and “non–thermal only” AGN. A significant fraction of FR–Is do have warm dust emission which could be attributed to hidden type–1 nuclei, a conclusion also anticipated on other grounds (e.g. Antonucci 2002a).

This work is based on observations made with the *Spitzer Space Telescope*, which is operated by the Jet Propulsion Laboratory, California Institute of Technology under a contract with NASA. Support for this work was provided by NASA through an award issued by JPL/Caltech. We have also made use of the NASA/IPAC Extragalactic Database (NED), which is operated by the Jet Propulsion Laboratory, California Institute of Technology, under contract with NASA. We thank Ann Wehrle for a critical reading of a previous version of this paper, and also Alan Marscher and Luis Ho for advice on specific issues. We are grateful to Marco Chiaberge for comments on a previous version of the paper and for newly measuring the optical compact core flux of 3C15. We are thankful for the critical comments of the referee which helped to improve the paper. This reaserch has made use of SDSS data products. Funding for the SDSS and SDSS-II has been provided by the Alfred P. Sloan Foundation, the Participating Institutions, the National Science Foundation, the U.S. Department of Energy, the National Aeronautics and Space Administration, the Japanese Monbukagakusho, the Max Planck Society, and the Higher Education Funding Council for England. The SDSS Web Site is <http://www.sdss.org/>.

Facilities: Spitzer (IRS)

A. Appendix: Examples for the subtraction of the star-forming template

Here we present additional plots on the subtraction of the star-formation component. The object 3C270 is already shown in Figs.5 and 9 while 3C83.1 as well as 3C272.1 can be found in Fig.6. This leaves 3C129, 3C386, and IC4296 as objects in which a significant correction due to emission from star formation was applied. We do not show objects which are clearly dominated by star formation in their MIR spectra (see Tab.2). We also do not show objects where the contributions from star formation – as traced by the PAH features – is very minor and thus only a very small correction was made (3C84, 3C120, NGC 6251, E1821+643; Tabs.2,3).

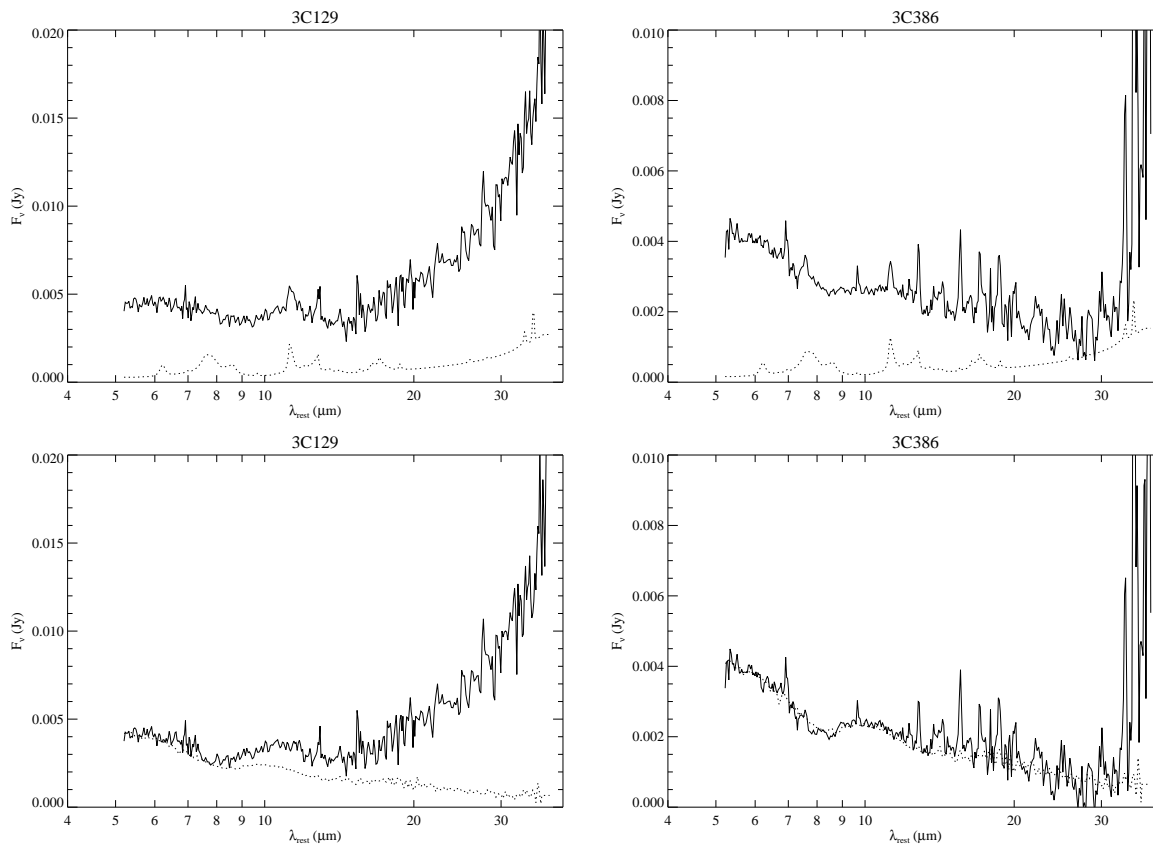


Fig. 13.— Subtraction of the star-forming template for 3C129 (*left*) and 3C386 (*right*). The top panel shows the observed spectrum with the scaled star-forming template. The bottom panel shows the corrected spectrum with a scaled spectrum of an early-type galaxy (NGC 1549).

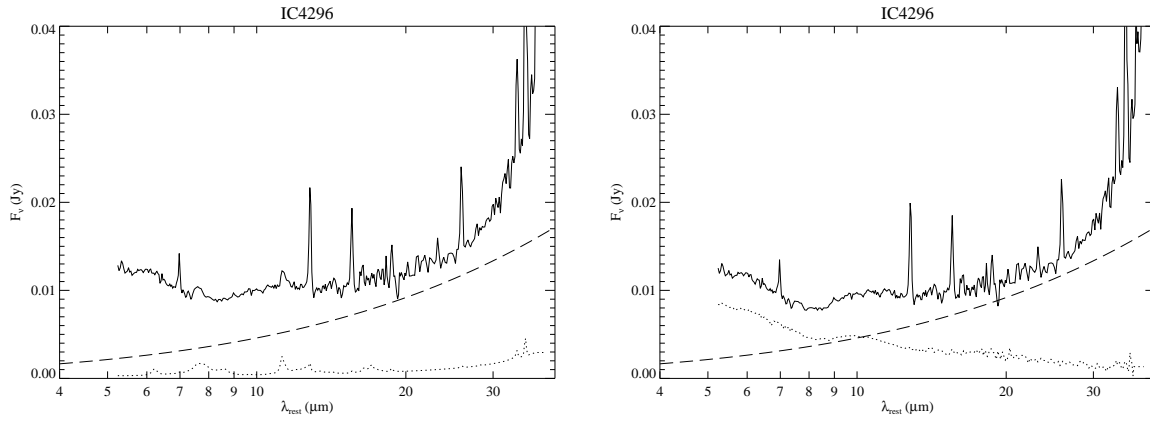


Fig. 14.— Subtraction of the star-forming template for IC4296. The panels are organized the same way as in Fig. 13. Here it becomes obvious what is mentioned in the note to Table 2: Due to the strong relative contribution from the synchrotron core (long-dashed line; Fig. 8) the scaling of the templates to *features* in the spectrum can result in overcorrections. Also, the steep slope at $\lambda > 30 \mu\text{m}$ hints at substantial emission from cold dust (which is supported by FIR measurements; Fig. 7) might influence the measurement at $30 \mu\text{m}$.

REFERENCES

- Antonucci, R. 1984, *ApJ*, 278, 499
- Antonucci, R. R. J., & Ulvestad, J. S. 1985, *ApJ*, 294, 158
- Antonucci, R. R. J. 1986, *ApJ*, 304, 634
- Antonucci, R. 1993, *ARA&A*, 31, 473
- Antonucci, R. 2002a, *Astrophysical Spectropolarimetry*, 151
- Antonucci, R. 2002b, *IAU Colloq. 184: AGN Surveys*, 284, 147
- Aretxaga, I., Terlevich, E., Terlevich, R. J., Cotter, G., & Díaz, Á. I. 2001, *MNRAS*, 325, 636
- Baars, J. W. M., Genzel, R., Pauliny-Toth, I. I. K., & Witzel, A. 1977, *A&A*, 61, 99
- Baldwin, J. A., Phillips, M. M., & Terlevich, R. 1981, *PASP*, 93, 5
- Balmaverde, B., & Capetti, A. 2006a, *A&A*, 447, 97
- Balmaverde, B., Capetti, A., & Grandi, P. 2006b, *A&A*, 451, 35
- Barth, A. J., Filippenko, A. V., & Moran, E. C. 1999, *ApJ*, 525, 673
- Barthel, P. D. 1989, *ApJ*, 336, 606
- Baum, S. A., et al. 1997, *ApJ*, 483, 178
- Begelman, M. C., Blandford, R. D., & Rees, M. J. 1984, *RvMP*, 56, 255
- Black, A. R. S., Baum, S. A., Leahy, J. P., Perley, R. A., Riley, J. M., & Scheuer, P. A. G. 1992, *MNRAS*, 256, 186
- Bundell, K. M., & Rawlings, S. 2001, *ApJ*, 562, 5
- Bower, G. A., et al. 2000, *ApJ*, 534, 189
- Brandl, B. R., et al. 2006, *ApJ*, 653, 1129
- Bressan, A., et al. 2006, *ApJ*, 639, 55
- Bridle, A. H., & Fomalont, E. B. 1978, *AJ*, 83, 704
- Bridle, A. H., Fomalont, E. B., & Cornwell, T. J. 1981, *AJ*, 86, 1294
- Bridle, A. H., & Perley, R. A. 1984, *ARA&A*, 22, 319
- Buchanan, C. L., Gallimore, J. F., O’Dea, C. P., Baum, S. A., Axon, D. J., Robinson, A., Elitzur, M., & Elvis, M. 2006, *AJ*, 132, 401
- Burch, S. F. 1977, *MNRAS*, 181, 599
- Burns, J. O. 1990, *AJ*, 99, 14
- Butcher, H. R., van Breugel, W., & Miley, G. K. 1980, *ApJ*, 235, 749
- Buttiglione, S., Capetti, A., Celotti, A., Axon, D. J., Chiaberge, M., Macchetto, F. D., & Sparks, W. B. 2009, *A&A*, 495, 1033
- Cao, X., & Rawlings, S. 2004, *MNRAS*, 349, 1419
- Capetti, A., Morganti, R., Parma, P., & Fanti, R. 1993, *A&AS*, 99, 407
- Capetti, A., Trussoni, E., Celotti, A., Feretti, L., & Chiaberge, M. 2000, *MNRAS*, 318, 493
- Capetti, A., Celotti, A., Chiaberge, M., de Ruiter, H. R., Fanti, R., Morganti, R., & Parma, P. 2002, *A&A*, 383, 104
- Capetti, A., Axon, D. J., Chiaberge, M., Sparks, W. B., Macchetto, F. D., Cracraft, M., & Celotti, A. 2007, *A&A*, 471, 137
- Cassaro, P., Stanghellini, C., Bondi, M., Dallacasa, D., della Ceca, R., & Zappalà, R. A. 1999, *A&AS*, 139, 601
- Chiaberge, M., Capetti, A., & Celotti, A. 1999, *A&A*, 300, 643
- Chiaberge, M., Celotti, A., Capetti, A., & Ghisellini, G. 2000b, *A&A*, 358, 104
- Chiaberge, M., Macchetto, F. D., Sparks, W. B., Capetti, A., & Martle, A. 2002, *ApJ*, 571, 247
- Chiaberge, M., Gilli, R., Capetti, A., & Macchetto, F. D. 2003, *ApJ*, 597, 166
- Cleary, K., Lawrence, C. R., Marshall, J. A., Hao, L., & Meier, D. 2007, *ApJ*, 660, 117
- Cohen, M. H., Ogle, P., Tran, H. D., Goodrich, R. W., & Miller, J. S. 1999, *AJ*, 118, 1963
- Condon, J. J., & Broderick, J. J. 1988, *AJ*, 96, 30

- Condon, J. J., Frayer, D. T., & Broderick, J. J. 1991, *AJ*, 101, 362
- Crane, P., et al. 1993, *AJ*, 106, 1371
- Dale, D. A., et al. 2005, *ApJ*, 633, 857
- Das, M., Vogel, S. N., Verdoes Kleijn, G. A., O’Dea, C. P., & Baum, S. A. 2005, *ApJ*, 629, 757
- De Robertis, M. M., & Yee, H. K. C. 1990, *AJ*, 100, 84
- Dicken, D., Tadhunter, C., Morganti, R., Buchanan, C., Oosterloo, T., & Axon, D. 2008, *ApJ*, 678, 712
- Dicken, D., Tadhunter, C., Axon, D., Morganti, R., Inskip, K. J., Holt, J., Delgado, R. G., & Groves, B. 2009, *ApJ*, 694, 268
- di Serego Alighieri, S., Cimatti, A., Fosbury, R. A. E., & Hes, R. 1997, *A&A*, 328, 510
- Doi, A., Kamenno, S., Kohno, K., Nakanishi, K., & Inoue, M. 2005, *MNRAS*, 363, 692
- Dulwich, F., Worrall, D. M., Birkinshaw, M., Padgett, C. A., & Perlman, E. S. 2007, *MNRAS*, 374, 1216
- Edge, D. O., Shakeshaft, J. R., McAdam, W. B., Baldwin, J. E., & Archer, S. 1959, *MNRAS*, 68, 37
- Evans, A. S., Mazzarella, J. M., Surace, J. A., Frayer, D. T., Iwasawa, K., & Sanders, D. B. 2005a, *ApJS*, 159, 197
- Evans, D. A., Hardcastle, M. J., Croston, J. H., Worrall, D. M., & Birkinshaw, M. 2005b, *MNRAS*, 359, 363
- Evans, D. A., Worrall, D. M., Hardcastle, M. J., Kraft, R. P., & Birkinshaw, M. 2006, *ApJ*, 642, 96
- Fanaroff, B. L., & Riley, J. M. 1974, *MNRAS*, 167, 31
- Ferrarese, L., Ford, H. C., & Jaffe, W. 1996, *ApJ*, 470, 444
- Ferrarese, L., & Ford, H. C. 1999, *ApJ*, 515, 583
- Giovannini, G., Feretti, L., Gregorini, L., & Parma, P. 1988, *A&A*, 199, 73
- Giovannini, G., Feretti, L., Venturi, T., Lara, L., Marcaide, J., Rioja, M., Spangler, S. R., & Wehrle, A. E. 1994, *ApJ*, 435, 116
- Giovannini, G., Taylor, G. B., Feretti, L., Cotton, W. D., Lara, L., & Venturi, T. 2005, *ApJ*, 618, 635
- Giozzi, M., Sambruna, R. M., & Brandt, W. N. 2003, *A&A*, 408, 949
- Giozzi, M., Sambruna, R. M., Brandt, W. N., Mushotzky, R., & Eracleous, M. 2004, *A&A*, 413, 139
- Golombek, D., Miley, G. K., & Neugebauer, G. 1988, *AJ*, 95, 26
- Govoni, F., Falomo, R., Fasano, G., & Scarpa, R. 2000, *A&A*, 353, 507
- Gower, A. C., & Hutchings, J. B. 1984, *AJ*, 89, 1658
- Haas, M., et al. 2004, *A&A*, 424, 531
- Haas, M., Siebenmorgen, R., Schulz, B., Krügel, E., & Chini, R. 2005, *A&A*, 442, 39
- Hansen, L., Jorgensen, H. E., & Norgaard-Nielsen, H. U. 1995, *A&A*, 297, 13
- Hardcastle, M. J., Alexander, P., Pooley, G. G., & Riley, J. M. 1996, *MNRAS*, 278, 273
- Hardcastle, M. J., Alexander, P., Pooley, G. G., & Riley, J. M. 1998, *MNRAS*, 296, 445
- Hardcastle, M. J., & Worrall, D. M. 2000, *MNRAS*, 314, 359
- Hardcastle, M. J., Birkinshaw, M., & Worrall, D. M. 2001, *MNRAS*, 326, 1499
- Hes, R., Barthel, P. D., & Fosbury, R. A. E. 1993, *Nature*, 362, 326
- Heywood, I., Blundell, K. M., & Rawlings, S. 2007, *MNRAS*, 381, 1093
- Hines, D. C., Eilek, J. A., & Owen, F. N. 1989, *ApJ*, 347, 713

- Ho, L. C., Filippenko, A. V., & Sargent, W. L. W. 1997, *ApJS*, 112, 315
- Ho, L. C., Filippenko, A. V., Sargent, W. L. W., & Peng, C. Y. 1997, *ApJS*, 112, 391
- Houck, J. R., et al. 2004, *ApJS*, 154, 18
- Jackson, N., & Browne, I. W. A. 1990, *Nature*, 343, 43
- Jackson, N., Sparks, W. B., Miley, G. K., & Machetto, F. 1993, *A&A*, 269, 128
- Jaffe, W., Ford, H. C., Ferrarese, L., van den Bosch, F., & O'Connell, R. W. 1993, *Nature*, 364, 213
- Jetha, N. N., Hardcastle, M. J., & Sakelliou, I. 2006, *MNRAS*, 368, 609
- Jones D. L., et al. 1986, *ApJ*, 305, 684
- Jones, D. L., & Wehrle, A. E. 1997, *ApJ*, 484, 186
- Jones, D. L., Wehrle, A. E., Meier, D. L., & Piner, B. G. 2000, *ApJ*, 534, 165
- Kaneda, H., Onaka, T., & Sakon, I. 2005, *ApJ*, 632, L83
- Kaneda, H., Onaka, T., Kitayama, T., Okada, Y., & Sakon, I. 2007, *PASJ*, 59, 107
- Kaneda, H., Onaka, T., Sakon, I., Kitayama, T., Okada, Y., & Suzuki, T. 2008, *ApJ*, 684, 270
- Kataoka, J., Leahy, J. P., Edwards, P. G., Kino, M., Takahara, F., Serino, Y., Kawai, N., & Martel, A. R. 2003, *A&A*, 410, 833
- Kauffmann, G., et al. 2003, *MNRAS*, 346, 1055
- Kellermann, K. I., Pauliny-Toth, I. I. K., & Williams, P. J. S. 1969, *ApJ*, 157, 1
- Kewley, L. J., Dopita, M. A., Sutherland, R. S., Heisler, C. A., & Trevena, J. 2001, *ApJ*, 556, 121
- Kewley, L. J., Groves, B., Kauffmann, G., & Heckman, T. 2006, *MNRAS*, 372, 961
- Kharb, P., Shastri, P., & Gabuzda, D. C. 2005, *ApJ*, 632, L69
- Killeen, N. E. B., Bicknell, G. V., & Ekers, R. D. 1986, *ApJ*, 302, 306
- Knapp, G. R., Guhathakurta, P., Kim, D.-W., & Jura, M. A. 1989, *ApJS*, 70, 329
- Knapp, G. R., Bies, W. E., & van Gorkom, J. H. 1990, *AJ*, 99, 476
- Knapp, G. R., & Patten, B. M. 1991, *AJ*, 101, 1609
- Kollatschny, W., Zetzl, M., & Dietrich, M. 2006, *A&A*, 454, 459
- Kollgaard, R. I., Wardle, J. F. C., Roberts, D. H., & Gabuzda, D. C. 1992, *AJ*, 104, 1687
- Kolman, M., Halpern, J. P., Shrader, C. R., & Filippenko, A. V. 1991, *ApJ*, 373, 57
- Kuehr, H., Witzel, A., Pauliny-Toth, I. I. K., & Nauber, U. 1981, *A&AS*, 45, 367
- Lacy, M., Rawlings, S., & Warner, P. J. 1992, *MNRAS*, 256, 404
- Laing, R. A., & Peacock, J. A. 1980, *MNRAS*, 190, 903
- Laing, R. A., Riley, J. M., & Longair, M. S. 1983, *MNRAS*, 204, 151
- Laing R. A., & Bridle, A. H. 1987, *MNRAS*, 228, 557
- Laing, R. A., Bridle, A. H., Parma, P., Feretti, L., Giovannini, G., Murgia, M., & Perley, R. A. 2008, *MNRAS*, 386, 657
- Lal, D. V., & Rao, A. P. 2004, *A&A*, 420, 491
- Landau, R., Jones, T. W., Epstein, E. E., Neugebauer, G., Soifer, B. T., Werner, M. W., Puschell, J. J., & Balonek, T. J. 1983, *ApJ*, 268, 68
- Landau, R., Golisch, B., Jones, T. J., et al. 1986, *ApJ*, 308, 78
- Lara, L., Giovannini, G., Cotton, W. D., Feretti, L., & Venturi, T. 2004, *A&A*, 415, 905
- Lawrence, C. R., Zucker, J. R., Readhead, A. C. S., Unwin, S. C., Pearson, T. J., & Xu, W. 1996, *ApJS*, 107, 541
- Leahy, J. P., & Perley, R. A. 1991, *AJ*, 102, 537

- Leahy, J. P., Black, A. R. S., Dennett–Thorpe, J., Hardcastle, M. J., Komissarov, S., Perley, R. A., Riley, J. M., & Scheuer, P. A. G. 1997, *MNRAS*, 291, 20
- Leeuw, L. L., Sansom, A. E., & Robson, E. I. 2000, *MNRAS*, 311, 683
- Leeuw, L. L., Sansom, A. E., Robson, E. I., Haas, M., & Kuno, N. 2004, *ApJ*, 612, 837
- Lewis, K. T., Eracleous, M., & Sambruna, R. M. 2003, *ApJ*, 593, 115
- Lister, M. L., & Homan, D. C. 2005, *AJ*, 130, 1389
- Lynds, R. 1971, *ApJ*, 168, L87
- Macchetto, F., et al. 1991, *ApJ*, 373, L55
- Madrid, J. P., et al. 2006, *ApJS*, 164, 307
- Martel, A. R., et al. 1998, *ApJ*, 496, 203
- Meisenheimer, K., Haas, M., Müller, S. A. H., Chini, R., Klaas, U., & Lemke, D. 2001, *A&A*, 372, 719
- Melnick, J., Gopal-Krishna, & Terlevich, R. 1997, *A&A*, 318, 337
- Miley, G. K., & Osterbrock, D. E. 1979, *PASP*, 91, 257
- Morganti, R., Killeen, N. E. B., & Tadhunter, C. N. 1993, *MNRAS*, 263, 1023
- Morganti, R., Oosterloo, T. A., Reynolds, J. E., Tadhunter, C. N., & Migenes, V. 1997, *MNRAS*, 284, 541
- Morganti, R., Oosterloo, T., Tadhunter, C. N., Aiudi, R., Jones, P., & Villar–Martin, M. 1999, *A&AS*, 140, 355
- Nagar, N. M., Wilson, A. S., & Falcke, H. 2001, *ApJ*, 559, L87
- Nieppola, E., Tornikoski, M., & Valtaoja, E. 2006, *A&A*, 445, 441
- O’Dea, C. P., & Owen, F. N. 1986, *ApJ*, 301, 841
- Ogle, P., Cohen, M. H., Miller, J. S., Tran, H. D., Fosbury, R. A. E., & Goodrich, R. W. 1997, *ApJ*, 482, 37
- Ogle, P., Whysong, D., & Antonucci, R. 2006, *ApJ*, 647, 161
- Ogle, P., Antonucci, R., & Whysong, D. 2007, in *ASP Conf. Ser. 373*, ed. L. C. Ho & J.–M. Wang (San Francisco: ASP), p. 578
- Okuda, T., Kohno, K., Iguchi, S., & Nakanishi, K. 2005, *ApJ*, 620, 673
- Owen, F. N. & Ledlow, M. J. 1994, in *ASP Conf. Ser. 54*, *The First Stromlo Symposium: The Physics of Active Galaxies*, ed. G. V. Bicknell, M. A. Dopita, & P. J. Quinn (San Francisco: ASP), 319
- Owen, F. N., Ledlow, M. J., & William, C. 1996, *AJ*, 111, 53
- Pedlar, A., Ghataure, H. S., Davies, R. D., Harrison, B. A., Perley, R., Crane, P. C., & Unger, S. W. 1990, *MNRAS*, 246, 477
- Pellegrini, S., Venturi, T., Comastri, A., Fabbiano, G., Fiore, F., Vignali, C., Morganti, R., & Trinchieri, G. 2003, *ApJ*, 585, 677
- Perley, R. A., Bridle, A. H., & Willis, A. G. 1984, *ApJS*, 54, 291
- Perlman, E. S., Sparks, W. B., Radomski, J., Packham, C., Fisher, R. S., Piña, R., & Biretta, J. A. 2001, *ApJ*, 561, 51
- Perlman, E. S., et al. 2006, *ApJ*, 651, 735
- Perlman, E. S., et al. 2007, *ApJ*, 663, 808
- Quillen, A. C., Almog, J., & Yukita, M. 2003, *AJ*, 126, 2677
- Quillen, A. C., et al. 2008, *ApJS*, 176, 39
- Rawlings, S., & Saunders, R. 1991, *Nature*, 349, 138
- Ricci, R., Prandoni, I., Gruppioni, C., Sault, R. J., & de Zotti, G. 2006, *A&A*, 445, 465
- Rinn, A. S., Sambruna, R. M., & Gliozzi, M. 2005, *ApJ*, 621, 167
- Sambruna, R. M., Chartas, G., Eracleous, M., Mushotzky, R. F., & Nousek, J. A. 2000, *ApJ*, 532, L91

- Sambruna, R. M., Gliozzi, M., Eracleous, M., Brandt, W. N., & Mushotzky, R. 2003, *ApJ*, 586, L37
- Shi, Y., et al. 2005, *ApJ*, 629, 88
- Shi, Y., Rieke, G. H., Hines, D. C., Gordon, K. D., & Egami, E. 2007a, *ApJ*, 655, 781
- Shi, Y., et al. 2007b, *ApJ*, 669, 841
- Shuder, J. M., & Osterbrock, D. E. 1981, *ApJ*, 250, 55
- Simpson, C., Ward, M., Clements, D. L., & Rawlings, S. 1996, *MNRAS*, 281, 509
- Simpson, C. 1998, *MNRAS*, 297, L39
- Skrutskie, M. F., et al. 2006, *AJ*, 131, 1163
- Smith, J. D. T., et al. 2007, *ApJ*, 656, 770
- Stickel, M., Lemke, D., Klaas, U., Krause, O., & Egner, S. 2004, *A&A*, 422, 39
- Strom, R. G., Willis, A. G., & Wilson, A. S. 1978, *A&A*, 68, 367
- Sturm, E., et al. 2006, *ApJ*, 653, L13
- Spinrad, H., Marr, J., Aguilar, L., & Djorgovski, S. 1985, *PASP*, 97, 932
- Spoon, H. W. W., Marshall, J. A., Houck, J. R., Elitzur, M., Hao, L., Armus, L., Brandl, B. R., & Charmandaris, V. 2007, *ApJ*, 654, 49
- Tadhunter, C. N., Morganti, R., di Serego-Alighieri, S., Fosbury, R. A. E., & Danziger, I. J. 1993, *MNRAS*, 263, 999
- Tadhunter, C. N., Morganti, R., Robinson, A., Dickson, R., Villar-Martin, M., & Fosbury, R. A. E. 1998, *MNRAS*, 298, 1035
- Tadhunter, C., Robinson, T. G., González Delgado, R. M., Wills, K., & Morganti, R. 2005, *MNRAS*, 356, 480
- Tadhunter, C., Dicken, D., Holt, J., Inskip, K., Morganti, R., Axon, D., Buchanan, C., González Delgado, R., Barthel, P., & van Bemmel, I. 2007, *ApJ*, 661, 13
- Tansley, D., Birkinshaw, M., Hardcastle, M. J., & Worrall, D. M. 2000, *MNRAS*, 317, 623
- Taylor, G. B., Perley, R. A., Inoue, M., Kato, T., Tabara, H., & Aizu, K. 1990, *ApJ*, 360, 41
- Taylor, G. B., Govoni, F., Allen, S. W., & Fabian, A. C. 2001, *MNRAS*, 326, 2
- Taylor, G. B., Gugliucci, N. E., Fabian, A. C., Sanders, J. S., Gentile, G., & Allen, S. W. 2006, *MNRAS*, 368, 1500
- Temi, P., Brighenti, F., & Matthews, W. G. 2007, *ApJ*, 660, 1215
- Trussoni, E., Capetti, A., Celotti, A., Chiaberge, M., & Feretti, L. 2003, *A&A*, 403, 889
- Urry, M., & Padovani, P. 1995, *PASP*, 107, 803
- Vallee, J. P. 1982, *AJ*, 87, 486
- van Bemmel, I. M., Dullemond, C. P., Chiaberge, M., & Macchetto, F. D. 2004, *astro-ph/0412374*
- van Breugel, W. & Jägers, W. 1982, *A&AS*, 49, 529
- Veilleux, S., & Osterbrock, D. E. 1987, *ApJS*, 63, 295
- Venturi, T., Castaldini, C., Cotton, W. D., Feretti, L., Giovannini, G., Lara, L., Marcaide, J. M., & Wehrle, A. E. 1995, *ApJ*, 454, 735
- Venturi, T., Morganti, R., Tzioumis, T., & Reynolds, J. 2000, *A&A*, 363, 84
- Walker, R. C., Benson, J. M., & Unwin, S. C. 1987, *ApJ*, 316, 546
- Weedman, D. W., et al. 2005, *ApJ*, 633, 706
- Werner, M. W., et al. 2004, *ApJS*, 154, 1
- Whysong, D., & Antonucci, R. 2001, *arXiv:astro-ph/0106381*
- Whysong, D., & Antonucci, R. 2004, *ApJ*, 602, 116
- Wills, K. A., Morganti, R., Tadhunter, C. N., Robinson, T. G., & Villar-Martin, M. 2004, *MNRAS*, 347, 771
- Wu, Q., Yuan, F., & Cao, X. 2007, *ApJ*, 669, 96
- Xu, C., O’Dea, C. P., & Biretta, J. A. 1999, *AJ*, 117, 2626

Xu, C., Baum, S. A., O'Dea, C. P., Wrobel, J. M.,
& Condon, J. J. 2000, AJ, 120, 2950

Zezas, A., Birkinshaw, M., Worrall, D. M., Peters,
A., & Fabbiano, G. 2005, ApJ, 627, 711

Zhao, J.-H., Sumi, D. M., Burns, J. O., & Duric,
N. 1993, ApJ, 416, 51

Zirbel, E. L., & Baum, S. A. 2003, AJ, 125, 1795